NORFLOXACIN ADSORPTION BY ACTIVATED CARBON FROM TURMERIC WASTE

Miss Nuttamon Vanichsetakul

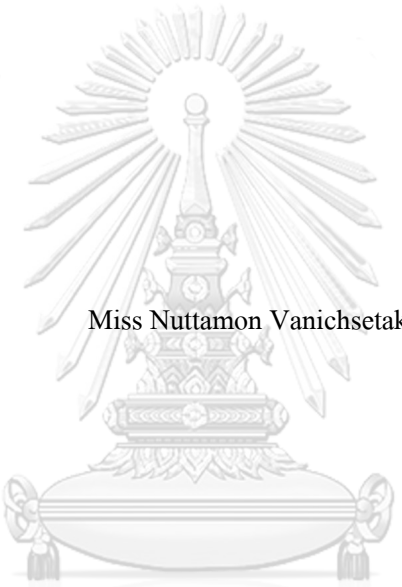

จุฬาลงกรณ์มหาวิทยาลัย
CHULALONGKORN UNIVERSITY

A Thesis Submitted in Partial Fulfillment of the Requirements

for the Degree of Master of Engineering in Chemical Engineering

Department of Chemical Engineering

FACULTY OF ENGINEERING

Chulalongkorn University

Academic Year 2021

Copyright of Chulalongkorn University

การดูดซับสารนอร์ฟลอกซาซินโดยถ่านกัมมันต์จากกากขมิ้นชัน

น.ส.นัทธมน วาณิชยเศรษฐกุล

จุฬาลงกรณ์มหาวิทยาลัย
Chulalongkorn University

วิทยานิพนธ์นี้เป็นส่วนหนึ่งของการศึกษาตามหลักสูตรปริญญาวิศวกรรมศาสตรมหาบัณฑิต
สาขาวิชาวิศวกรรมเคมี ภาควิชาวิศวกรรมเคมี
คณะวิศวกรรมศาสตร์ จุฬาลงกรณ์มหาวิทยาลัย
ปีการศึกษา 2564
ลิขสิทธิ์ของจุฬาลงกรณ์มหาวิทยาลัย

Thesis Title	NORFLOXACIN ADSORPTION BY ACTIVATED CARBON FROM TURMERIC WASTE
By	Miss Nuttamon Vanichsetakul
Field of Study	Chemical Engineering
Thesis Advisor	Assistant Professor NATTAPORN TONANON, D.Eng.

Accepted by the FACULTY OF ENGINEERING, Chulalongkorn University in Partial Fulfillment of the Requirement for the Master of Engineering

..... Dean of the FACULTY OF ENGINEERING

(Professor SUPOT TEACHAVORASINSKUN, D.Eng.)

THESIS COMMITTEE

..... Chairman

(Professor JOONGJAI PANPRANOT, Ph.D.)

..... Thesis Advisor

(Assistant Professor NATTAPORN TONANON, D.Eng.)

..... Examiner

(Professor PAISAN KITTISUPAKORN, Ph.D.)

..... Examiner

(Chanchana Thanachayanont, Ph.D.)

จุฬาลงกรณ์มหาวิทยาลัย
CHULALONGKORN UNIVERSITY

นัทธมน วาณิชยเศรษฐกุล : การดูดซับสารนอร์ฟลอกซาซินโดยถ่านกัมมันต์จากกากขมิ้นชัน.
(NORFLOXACIN ADSORPTION BY ACTIVATED CARBON FROM TURMERIC WASTE)
อ.ที่ปรึกษาหลัก : ผศ. ดร.ณัฐพร โทณานนท์

ทุกวันนี้การใช้งานอย่างแพร่หลายของยาแผนปัจจุบันและความไม่มีประสิทธิภาพของระบบบำบัดน้ำเสียแบบทั่วไปทำให้เกิดปัญหาการปนเปื้อนยาปฏิชีวนะในสิ่งแวดล้อมโดยเฉพาะในประเทศที่มีรายได้น้อย ยาปฏิชีวนะในสิ่งแวดล้อมสามารถมีปฏิสัมพันธ์กับแบคทีเรียตามธรรมชาตินำไปสู่การดื้อยาชนิดนั้นๆ นอกจากนี้ยาปฏิชีวนะยังรบกวนความสมดุลของระบบนิเวศส่งผลกระทบไปถึงสิ่งมีชีวิตหลายชนิด นอร์ฟลอกซาซินเป็นยาปฏิชีวนะที่ใช้กันทั่วไปในประเทศไทย อีกทั้งยังมีการตรวจพบการปนเปื้อนของนอร์ฟลอกซาซินในแม่น้ำบางปะกง กระบวนการดูดซับเป็นวิธีที่ถูกและมีประสิทธิภาพในการกำจัดยาปฏิชีวนะของจากน้ำทิ้ง ถ่านกัมมันต์เป็นตัวดูดซับที่ใช้กันอย่างแพร่หลายในกระบวนการดูดซับเนื่องด้วยคุณสมบัติความเป็นรูพรุนของถ่านกัมมันต์ ของเหลือทิ้งทางการเกษตรเป็นตัวเลือกของวัตถุดิบทำถ่านกัมมันต์ที่ราคาถูกและหมุนเวียนได้ ของเหลือทิ้งการการเกษตรที่ใหม่และน่าสนใจสำหรับการเป็นแหล่งคาร์บอนให้กับถ่านกัมมันต์คือกากขมิ้นชัน ซึ่งสะอาดและมีปริมาณมาก ถ่านกัมมันต์จากกากขมิ้นชันถูกกระตุ้นด้วยสารเคมีเป็นมิตรต่อสิ่งแวดล้อม แคลเซียมคลอไรด์ ภายใต้บรรยากาศไนโตรเจนที่อุณหภูมิ 500-900 °C (TWAC500-900) พบว่าอุณหภูมิการสังเคราะห์ที่ดีที่สุดคือ 700 °C คาร์บอนที่ได้ (TWAC700) มีโครงสร้างแกรไฟต์เกิดขึ้นบางส่วนและพื้นผิวประกอบไปด้วยหมู่ฟังก์ชัน C ≡ C, C = O, และ C – H สมบัติรูพรุนของ TWAC มีดังนี้ พื้นที่ผิวจำเพาะ 334 m2/g, ปริมาตรรูพรุนมีโซพอร์ที่ค่อนข้างสูง 0.362 cm3/g, และปริมาตรรูพรุนไมโครพอร์ 0.0954 cm3/g. TWAC700 มีประสิทธิภาพการกำจัดนอร์ฟลอกซาซินสูง 96.1% และมีประสิทธิภาพการดูดสูงสุดแบบชั้นเดียว 41.7 mg/g การดูดซับเป็นแบบแลงเมียร์ซึ่งอธิบายถึงการดูดซับแบบชั้นเดียวบนพื้นผิวเนื้อเดียว ทั้งนี้ถ่านกัมมันต์จากกากขมิ้นชันส่งเสริมโมเดลธุรกิจ BCG โดยการเพิ่มมูลค่าให้กับของเหลือทิ้งทางการเกษตรและในเวลาเดียวกันก็ให้ถ่านกัมมันต์ชนิดใหม่เพื่อการดูดซับยาปฏิชีวนะตกค้างในระบบบำบัดน้ำเสียด้วยกระบวนการดูดซับ

จุฬาลงกรณ์มหาวิทยาลัย
Chulalongkorn University

สาขาวิชา	วิศวกรรมเคมี	ลายมือชื่อนิสิต .....
ปีการศึกษา	2564	ลายมือชื่อ อ.ที่ปรึกษาหลัก .....

6270137221 : MAJOR CHEMICAL ENGINEERING

KEYWORD: Turmeric, ACTIVATED CARBON, Adsorption, Norfloxacin

Nuttamon Vanichsetakul : NORFLOXACIN ADSORPTION BY ACTIVATED CARBON FROM TURMERIC WASTE. Advisor: Asst. Prof. NATTAPORN TONANON, D.Eng.

In recent years, extensive use of modern medicines and incompetency of conventional wastewater treatment systems have led to contamination of antibiotics in the environment especially in lower income countries. Antibiotics could interact with bacteria in the environment forming resistance to the medicine. Antibiotics also disrupt the balance of ecosystems affecting various lifeforms. Norfloxacin is a common antibiotic in Thailand with reported levels of contamination in Bang Pakong River. Adsorption process is a cheap and effective approach to remove antibiotics from wastewater effluent. Activated carbon is a common adsorbent in adsorption process due to its porous properties. Agricultural waste presents as an inexpensive and renewable precursor for activated carbons. Turmeric waste is an abundant and clean agricultural waste that is a novel activated carbon precursor. Turmeric waste activated carbon was prepared by the environmentally friendly $CaCl_2$ under nitrogen atmosphere at 500-900 °C (TWAC500-900). The optimal carbonization temperature was 700 °C. TWAC700 was partly graphitized, and the surface contained C ≡ C, C = O, and C – H functional groups. Porosity of TWAC700 included BET surface area 334 m^2/g, considerably high mesopore volume 0.362 cm^3/g, and micropore volume 0.0954 cm^3/g. TWAC700 showed high Norfloxacin removal efficiency (96.1%) with maximum monolayer adsorption capacity at 41.7 mg/g. The adsorption isotherm was in accordance with the Langmuir adsorption model which describes the monolayer adsorption on homogeneous surface. Turmeric waste activated carbon supports bio-circular-green economy model by adding value to agricultural waste, at the same time providing a new activated carbon for antibiotic residue removal in wastewater through adsorption process.

จุฬาลงกรณ์มหาวิทยาลัย
CHULALONGKORN UNIVERSITY

Field of Study:	Chemical Engineering	Student's Signature .....
Academic Year:	2021	Advisor's Signature .....

ACKNOWLEDGEMENTS

I would like to acknowledge and give my thanks to my advisor Asst. Prof. Dr. Nattaporn Tonanon who made this work possible. Her guidance and advice carried me through all the stages of writing my thesis. I would also like to thank my committee members for letting my defense be an enjoyable moment, and for your brilliant comments and suggestions, thanks to you.

I would also like to give special thanks to my family as a whole for their continuous support and understanding when undertaking my research and writing my project.

Nuttamon Vanichsetakul

จุฬาลงกรณ์มหาวิทยาลัย
CHULALONGKORN UNIVERSITY

TABLE OF CONTENTS

Page

ABSTRACT (THAI) iii

ABSTRACT (ENGLISH) iv

ACKNOWLEDGEMENTS v

TABLE OF CONTENTS vi

LIST OF TABLES x

LIST OF FIGURES xii

Chapter 1 14

1.1 Background and Motivations 14

1.2 Objectives 16

1.3 Scopes 17

1.4 Expected outcomes 17

Chapter 2 18

2.1 Turmeric 18

2.2 Norfloxacin 20

2.2.1 NOR contamination in the environment 20

2.2.2 Studied adverse effect of NOR in the environment 26

2.3 Activated carbon 28

2.4 Biomass and agricultural waste 30

2.5 Carbonization process 31

2.6 Activation process 31

2.6.1 Chemical activation 31

จุฬาลงกรณ์มหาวิทยาลัย
CHULALONGKORN UNIVERSITY

2.6.2 Physical activation....32
2.7 Adsorption....33
2.7.1 Types of adsorption....34
2.8 Adsorption isotherm models....35
2.8.1 Langmuir isotherm model....35
2.8.2 Freundlich isotherm model....36
2.8.3 Dubinin-Radushkevitch (D-R) isotherm model....36
2.9 Adsorption kinetics models....37
2.9.1 Pseudo first order model (PFO)....37
2.9.2 Pseudo second order model (PSO)....38
2.9.3 Elovich model....38
2.9.4 Intra-particle diffusion model (IPD)....39
2.10 Adsorption thermodynamics....39
2.11 Activated carbon from turmeric waste....40
2.12 Norfloxacin adsorption....40
Chapter 3....44
3.1 Materials....44
3.1.1 Turmeric waste (TW)....44
3.1.2 Chemicals....44
3.1.3 Furnace....45
3.2 Methodology....46
3.2.1 Turmeric waste pretreatment....46
3.2.2 Calcium chloride impregnation....46
3.2.3 Turmeric waste activated carbon synthesis....47

จุฬาลงกรณ์มหาวิทยาลัย
Chulalongkorn University

3.2.4 Acid washing 47

3.2.5 Turmeric waste biochar synthesis 48

3.3 Characterization of turmeric waste and turmeric waste activated carbon (TWAC) 49

3.3.1 Thermogravimetric analysis 49

3.3.2 Field-emission electron scanning microscope and energy dispersive X-ray spectrometer 49

3.3.3 Nitrogen adsorption-desorption apparatus 49

3.3.4 X-ray diffractometer 49

3.3.5 Raman spectroscopy 50

3.3.6 Fourier transform infrared spectrophotometer 50

3.4 Norfloxacin adsorption 52

3.4.1 UV-vis spectrophotometer 52

3.4.2 Effect of carbon dosage 52

3.4.3 Effect of initial concentration 52

3.4.4 Adsorption equilibrium 53

3.4.5 Adsorption kinetics 53

3.4.6 Thermodynamics of adsorption 53

Chapter 4 54

4.1 Characteristic of turmeric waste 54

4.1.1 Thermal stability of turmeric waste and calcium chloride impregnated turmeric waste 54

4.2 Turmeric waste activated carbon synthesis 56

4.2.1 N_2 adsorption-desorption isotherms and porosity of turmeric waste activated carbon 56

4.2.2 Crystalline structure and amorphous structure 65

4.2.3 Carbon structure by Raman spectroscopy 66

จุฬาลงกรณ์มหาวิทยาลัย
CHULALONGKORN UNIVERSITY

4.2.4 Morphology and surface texture 68

4.2.5 Surface functional groups.....72

4.3 Norfloxacin adsorption 73

4.3.1 Effect of carbon dosage.....73

4.3.2 Effect of initial concentration.....74

4.3.3 Adsorption equilibrium 75

4.3.4 Adsorption kinetics 78

4.3.5 Thermodynamics of adsorption.....81

4.3.6 TWAC as NOR adsorbent compared to other biomass-based materials 83

Chapter 5 87

5.1 Activated carbon synthesis 87

5.2 Norfloxacin adsorption by activated carbon 88

Nomenclature 89

Appendix.....92

REFERENCES 101

VITA 110

จุฬาลงกรณ์มหาวิทยาลัย
Chulalongkorn University

LIST OF TABLES

Page

Table 1 Statistics of turmeric cultivation in 2018 [5] 18

Table 2 List of the biggest turmeric exporters and export value in 2019 [8] 19

Table 3 List of NOR contaminations in the WWTP discharge and in the environment.....24

Table 4 NOR experimental properties [28] 28

able 5 Structure and dimension of organic pollutant compounds [30] 29

Table 6 List of other adsorbents in literature and their NOR adsorption capacities 42

Table 7 Chemicals involved in this research and details 44

Table 8 Synthesis conditions of the prepared activated carbon and biochar from turmeric waste 48

Table 9 Porosity and isotherm characteristics of TWB and TWAC500-900 57

Table 10 Various activated carbon from lignocellulosic materials and their porosity 61

Table 11 Chemical compositions of TWAC700 characterized by SEM-EDX.....71

Table 12 Langmuir, Freundlich, and D-R isotherm parameters for NOR adsorption 76

Table 13 Pseudo-first-order (PFO), pseudo-second-order (PSO), and Elovich kinetic parameters for NOR adsorption.....79

Table 14 Intraparticle diffusion parameters 80

Table 15 Langmuir adsorption isotherm parameters at 20, 30, 40 °C 82

Table 16 NOR adsorption thermodynamics parameters 82

Table 17 List of group 3 biomass-based adsorbents and group 4 commercial activated carbons from Table 6 and their NOR adsorption capacities compared to this work.....86

Table 18 Lignocellulosic composition of turmeric waste 92

Table 19 Effect of carbon dosage, 25 °C, 200 rpm, 24 h (section 4.3.1).....98

จุฬาลงกรณ์มหาวิทยาลัย
Chulalongkorn University

Table 20 Effect of initial concentration and equilibrium of adsorption, 25 °C, 200 rpm, 24 h (section 4.3.2 – 4.3.3).....98

Table 21 Adsorption kinetics 25 °C, 200 rpm (section 4.3.4) 99

Table 22 Thermodynamics of adsorption, 200 rpm, 24 h (section 4.3.5).....100

จุฬาลงกรณ์มหาวิทยาลัย
CHULALONGKORN UNIVERSITY

LIST OF FIGURES

Page

Figure 1 Chemical structures of curcuminoids 19

Figure 2 Major sources of antibiotic in the environment (Modified from [18]).....21

Figure 3 2-D chemical structure of NOR.....27

Figure 4 3-D chemical structure and dimension of NOR 27

Figure 5 Molecular structure of NOR and its ionic forms as a function of pH [27].....28

Figure 6 Structure of cellulose.....30

Figure 7 Structure of hemicellulose [31] 30

Figure 8 Structure of lignin [32] 31

Figure 9 Activated carbon synthesis from biomass via chemical and physical activation flowchart 33

Figure 10 Transport processes during adsorption by a porous adsorbent [38] 34

Figure 11 Turmeric waste process 44

Figure 12 Schematic diagram of the furnace 45

Figure 13 Preparation of turmeric waste activated carbon 47

Figure 14 Flowchart of TWAC500-900 synthesis and characterization 51

Figure 15 Thermogravimetric analysis (TGA) of turmeric waste (TW) and $CaCl_2$ impregnated turmeric waste (TW-$CaCl_2$) 54

Figure 16 Derivative thermogravimetry (DTG) of TW and TW-$CaCl_2$ 55

Figure 17 N_2 adsorption and desorption isotherms at 77K of TWAC500-900 and TWB700 58

Figure 18 Mesopore size distribution of TWAC700 59

Figure 19 X-ray diffraction (XRD) patterns of TWAC500-900.....65

จุฬาลงกรณ์มหาวิทยาลัย
Chulalongkorn University

Figure 20 Raman spectra of TWAC500-900 66

Figure 21 SEM images of TWAC500 – 900 at different magnifications 68

Figure 22 FTIR spectra of TWAC700 72

Figure 23 Effect of carbon dosage on the %removal and q_e of NOR 73

Figure 24 Effect of C_0 (initial concentration) on the %removal and q_e of NOR 74

Figure 25 Isotherm fitting curves for NOR adsorption onto TWAC700 and experimental data ..75

Figure 26 R_L value across C_0 (initial concentration) = 0 – 200 mg/l 77

Figure 27 Kinetic models fitting curves for NOR adsorption onto TWAC700 and experimental data 78

Figure 28 Intraparticle diffusion model regression for NOR adsorption onto TWAC700 79

Figure 29 Langmuir isotherm fitting curves for NOR adsorption at 20 – 40 °C, C_0 = 20 – 80 mg/l 81

Figure 30 Plot of $\ln(K_c)$ versus 1/T (K^{-1}) 82

Figure 31 Carbokarn's commercial activated carbon grades [76] 84

Figure 31 Yield percentage of TWAC500 - 900 at different carbonization temperature 92

Figure 32 Initial pH and change in pH plot to determine pH_{pzc} of TWAC700 95

Figure 33 UV-Visible absorbance spectrum of standard NOR solution 1-10 mg/l 96

Figure 34Calibration plot of Norfloxacin concentration and absorbance at wavelength 277 nm .96

Figure 35 q_e of NOR adsorption using TWAC500-900 and TWB700 at C_0 = 25 mg/l 97

Figure 36 q_e of NOR adsorption using TWAC500-800 and TWB700 at C_0 = 10 mg/l 97

จุฬาลงกรณ์มหาวิทยาลัย
Chulalongkorn University

Chapter 1

Introduction

1.1 Background and Motivations

Global increase in population size and improved access to medical care have led to 26.2 percent increase in antibiotic use from the last 15 years [1]. Norfloxacin (NOR) is a common antibiotic used to treat urinary tract infections (UTIs) and diarrhea. NOR is a popular antibiotic in Thailand. NOR is usually prescribed by doctors, but people can also buy it from any pharmacy without prescriptions. Similar to other medicines, NOR is not completely metabolized in the human body with 30% of the dose excreted unchanged in urine in the first 24 h after administration [2]. Antibiotic is a pharmaceutical and personal care product (PPCP) which in recent years has been categorized as an emerging pollutant (EP). EP refers to a group of chemical compounds that are not regulated by law and their adverse effect on the environment is not fully known. In NOR case, hospital and municipal wastewater treatment system cannot effectively remove NOR in effluent leading to contamination in surface and ground water. In Thailand, 1.79-20.75 μg/l of NOR contamination was found in Bang Pakong River. Locating upstream of the collection points was a large hospital "Chao Phraya Abhaibhubejhr Hospital" where 5.04 μg/l of NOR was found in the wastewater treatment effluent. Another smaller hospital "Bang Pakong Hospital" had 2.53 μg/l of NOR contamination after treatment as well [3]. The reported levels of NOR in Bang Pakong River was enough to negatively affect organisms in the water. By nature, NOR being an antibiotic, it interferes with bacteria both in human body and outside. NOR is found to interact with degradation of other harmful chemicals such as herbicides allowing them to exist in water longer than normal [4]. Therefore, the danger of NOR in the environment does not come solely from NOR toxicity but from other chemicals as well. At present, there is no specific regulation of the acceptable level of NOR in wastewater treatment facility outputs in Thailand.

จุฬาลงกรณ์มหาวิทยาลัย
CHULALONGKORN UNIVERSITY

Typically, wastewater treatment systems are divided into 3 parts (i) primary treatment to remove larger solid particles, (ii) secondary treatment which is a biological process to degrade organic compounds, and (iii) tertiary treatment where leftover phosphates, nitrates, and other compounds are removed. Since many of the conventional secondary wastewater treatment techniques such as activated sludge and oxidation ditch, are incapable of completely treating NOR, an improvement to the system is needed. Adsorption process could be easily added as a tertiary step to catch all the leftover antibiotics. Commercial activated carbon is a common but costly adsorbent, so a lot of research has focused on finding low-cost adsorbents such as activated carbon from agricultural waste.

Turmeric is a traditional Thai herb with various medicinal properties including antimicrobial activity, and antibacterial activity in gastric system and skin. These properties are due to its active chemical “curcuminoids”; thus, turmeric has gained tremendous popularity in recent years. Products like turmeric essential oil and especially turmeric extract capsules are sold in almost every pharmacy. This high demand for turmeric products leads to high production creating waste from the discarded part of turmeric rhizome after extraction. This waste currently has no destination except for disposal. Turmeric waste presents some attractive features for being a raw material including low cost, abundance, easy collection from one location, and it is clean from being through a food-grade process. In an average production year, a turmeric product manufacturer can create up to 54 wet metric tons of turmeric residue. Turmeric waste is considered an agricultural waste that is rich in cellulose, hemicellulose, and lignin.

From the abovementioned reasons, turmeric waste presented as a potential activated carbon precursor due to its lignocellulosic structure and ease of collection. The obtained turmeric waste activated carbon would also be the solution to NOR contamination as the carbon could be conditioned to effectively adsorb NOR from wastewater. In conclusion, preparation of turmeric waste activated carbon was proposed in this work and to further explore turmeric waste activated carbon’s potential as NOR adsorbent.

1.2 Objectives

1. Value adding of turmeric waste
2. To study Norfloxacin adsorption capacity and characteristic by the prepared activated carbon

จุฬาลงกรณ์มหาวิทยาลัย
Chulalongkorn University

1.3 Scopes

Part 1 Activated carbon synthesis from turmeric waste

- Synthesis of activated carbon from turmeric waste under nitrogen atmosphere by chemical activation through impregnation with calcium chloride (ratio $CaCl_2$: turmeric waste = 1:1). Gas flow rate 100 cm^3/min, heating rate 10 °C/min, 2 h.
- Variable: carbonization temperature 500 - 900 °C

Part 2 Norfloxacin adsorption by the activated carbon obtained from part 1

- Batch adsorption experiments divided into 5 parts

1. Effect of carbon dosage, 0.25 - 3 g/l, initial Norfloxacin concentration 10 mg/l, temperature 25 °C, 24 h
2. Effect of initial concentration, 10 - 200 mg/l, temperature 25 °C, 24 h
3. Adsorption equilibrium, initial Norfloxacin concentration 5 - 200 mg/l, temperature 25 °C, 24 h
4. Adsorption kinetics, time 0 - 72 h, initial Norfloxacin concentration 40 mg/l, temperature 25 °C
5. Adsorption thermodynamics, temperature 20 - 40°C, initial Norfloxacin concentration 20 - 80 mg/l, 24 h

จุฬาลงกรณ์มหาวิทยาลัย
Chulalongkorn University

1.4 Expected outcomes

- a method to add value to turmeric waste
- a mean to treat antibiotic contaminated water via adsorption using activated carbon synthesized from turmeric waste

Chapter 2

Theory and Literature Review

2.1 Turmeric

Turmeric, scientific name *Curcuma longa* Linn., belongs to the Zingiberaceae family. Turmeric is commonly grown in South Asia and Southeast Asia. In Thailand, there are 4,431 Rais (ไร่) of turmeric cultivation land. In 2018, 3,462,950 kg of fresh turmeric rhizomes are grown in total. Statistics of turmeric cultivation in Thailand are shown in Table 1 in descending order below.

Table 1 Statistics of turmeric cultivation in 2018 [5]

Province	Cultivation area (Rai)	Harvest (kg)
Kanchanaburi (กาญจนบุรี)	2,570	2,523,000
Prachinburi (ปราจีนบุรี)	419	690,000
Surat Thani (สุราษฎร์ธานี)	386	-
Phang-Nga (พังงา)	357	-
Nakhon Si Thammarat (นครศรีธรรมราช)	113	80

จุฬาลงกรณ์มหาวิทยาลัย
Chulalongkorn University

The biggest turmeric producer and exporter is India. In 2018, India's highest producer state Telangana harvested 294,560 metric tons. The runner ups Maharashtra and Tamil Nadu produced 190,090 and 116,00 metric tons, respectively [6]. Turmeric export value of each country is shown in Table 2.

Turmeric extract can be divided into two types: essential oil and curcuminoids. Essential oil is yellow, found abundantly in the root and rhizome. Curcuminoids are a group of active compounds consisting of curcumin, demethoxycurcumin, and bisdemethoxycurcumin. Their

chemical structures are illustrated in Fig. 1. Turmeric extract is widely known for its medicinal properties for instance antimicrobial activity, and antibacterial activity in gastric system and skin [7].

Table 2 List of the biggest turmeric exporters and export value in 2019 [8]

Country	Export value (million USD)
India	194.35
UK	4.91
USA	4.66
Germany	4.47
Spain	2.64
Belgium	1.69

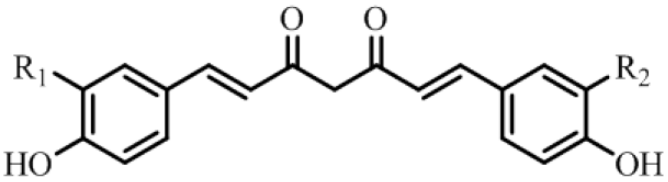

Curcumin; $R_1 = R_2 = OCH_3$

Demethoxycurcumin; $R_1 = H$, $R_2 = OCH_3$

Bisdemethoxycurcumin; $R_1 = R_2 = H$

Figure 1 Chemical structures of curcuminoids

Apart from its active compounds, turmeric contains cellulose, hemicellulose, and lignin. Turmeric waste, the residue of curcumin extraction process, was used as a precursor to isolate cellulose nanofiber through hydrolysis and high-pressure homogenization process. The obtained nanofiber retained turmeric's antimicrobial property against *Bacillus cereus*, *Escherichia Coli*,

Salmonella typhimurium, and *Staphylococcus aureus* bacteria [9]. The nanofiber was also crosslinked with chitosan and starch from potato and cassava to form a nanocomposite film [10].

2.2 Norfloxacin

Norfloxacin belongs to the Fluoroquinolone antibiotic group. Other medicines in this group include Ciprofloxacin, Levofloxacin, and gatifloxacin. It is primarily used to treat urinary tract infections and diarrhea from bacterial infections. Norfloxaxin has a direct effect on *Echerichia coli*, E coli. in short, which causes acute diarrhea. The mode of action is through inbitition of DNA gyrase enzyme in bacterias which is essential to bacteria DNA production preventing bateria from multiplication [11].

In Thailand, NOR is categorized into category A (บัญชี ก) in Thailand National List of Essential Medicines (NLEM) meaning that the medicine is the standard one that is used to treat common health issues with sufficient evidence and experience in Thailand, and that it would be the first medicine of choice [12]. Pharmacies normally have NOR readily available, and purchase can be made without a prescription. NOR exists in only an oral pill form unlike its counterpart Ciprofloxacin which comes in the form of oral pills and injections administered by a nurse.

จุฬาลงกรณ์มหาวิทยาลัย
CHULALONGKORN UNIVERSITY

2.2.1 NOR contamination in the environment

The extent of negative effect of NOR on the environment has not been fully understood yet as NOR is categorized as an emerging pollutant. Emerging pollutants are a group of chemical compounds that are not commonly monitored in the environment and have recently been identified as dangerous to the environment, and consequently to the health of human beings [13, 14].

NOR is rather stable and recalcitrant to degradation in the environment from its aromatic structure [15, 16]. NOR and other antibiotics are considered EPs of high concern because not only do their cumulative toxic effect on the environment not fully known but their continued existence

in growing amount promotes the development of bacteria resistance. Futhermore, because of their antimicrobial nature, antibiotic can alter the biodiversity in aquatic eosystems as well as interfering with the microorganisms in wastewater treatment process [17].

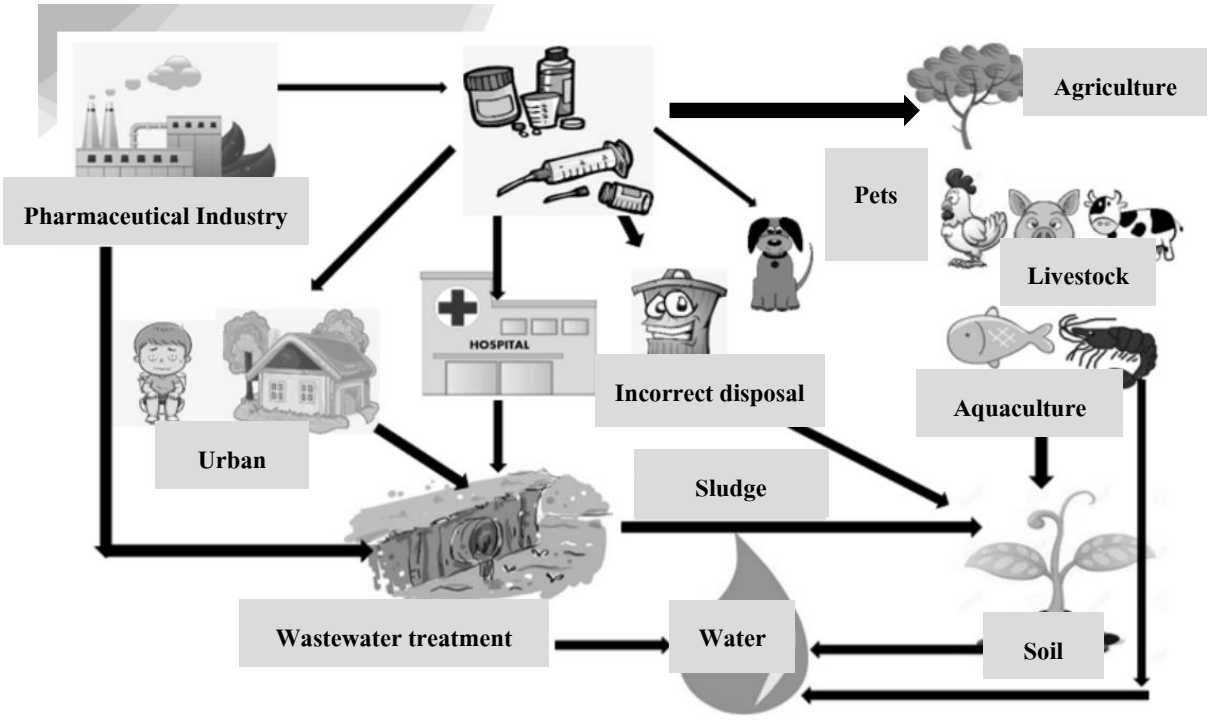

Figure 2 Major sources of antibiotic in the environment (Modified from [18])

There are several ways that NOR and other antibiotics can enter the water environment as illustrated in Fig. 2. The major contaminations came from two sources which are residues in hospital and pharmaceutical manufacturing wastewater. The contamination levels could go up to 100-500 mg/l in some cases [19]. It is evident that wastewater treatment plants (WWTPs) in many countries still cannot effectively remove NOR and other antibiotics from their effluent. In a developed country, Finland, a population of 1,000 individuals was estimated to create 36 ± 48 mg of NOR per day in wastewater influent. WWTPs would treat NOR and bring the contamination level down to 2 ± 8 mg per day per 1,000 people, thus leaving a good amount of NOR in the effluent [20].

There were also reports of significantly higher concentrations of NOR in water bodies downstream of pharmaceutical factories and WWTPs than upstream, and accumulation in the

nearby sediment. Patanchery Enviro Tech Ltd. (PETL) is a WWTP for 90 bulk pharmaceutical manufacturers in Patancheru, India, treating 1,500 m^3 of wastewater per day. NOR was found in the effluent of the plant at 25,000 ng/l. A lake locating upstream of PETL detected various medicine contamination including NOR 60,000 – 520,000 ng/l. Another lake upstream of PETL contained 91,000 – 200,000 ng/l of NOR. Moreover, up to 31 ng/l of NOR was found in a groundwater well in a nearby village. Downstream of the WWTP is Isakavagu-Nakkavagu River where up to 4,700 ng/l of NOR was detected [21].

A study in Kenya investigated the contamination of antibiotics including NOR in WWTP effluent, surface water, and river sediment. The Machakos WWTP in Machakos town, Kenya utilized waste stabilization ponds for wastewater treatment providing for 7.6% of the population of 50,753. The samples were collected twice during the year: in January, and in September (most arid month). NOR was found in the WWTP effluent in aqueous phase and suspended particulate matter phase at 4.2 μg/l and 82,267 μg/kg, respectively. There was an increase in NOR concentration in the Mitheu river 500 meters upstream and downstream of the WWTP discharge point. In September, NOR upstream and downstream concentrations were 1.6 μg/l and 4.9 μg/l respectively. In January the concentrations were lower, NOR upstream and downstream were 0.6 μg/l and 2.2 μg/l, respectively [22]. It can be concluded that especially in lower income countries, the effective mean to remove NOR from wastewater is lacking.

จุฬาลงกรณ์มหาวิทยาลัย
CHULALONGKORN UNIVERSITY

In Thailand, large hospitals, such as Chao Phraya Abhaibhubejhr Hospital detected 5.04 μg/l of NOR in hospital wastewater after the activated sludge oxidation ditch process. In Bang Pakong Hospital, a small hospital, 2.53 μg/l of NOR was found following the oxidation pond. A pig farm in the same area reported 39.2 μg/l of NOR in their discharge water. Both hospitals and the pig farm are located near Bang Pakong River where during the rainy season 1.79 - 20.75 μg/l of NOR was detected [3].

Another method to keep track of EPs in the environment is through biomonitoring organisms. Bivalves are common biomonitoring organisms because they feed by filtering food suspended in water. They retain 90% of the compounds that go into their bodies allowing them to

have information about the concentration levels that they live in. Many of the bivalves are also seafood meaning whatever contaminants they have in their bodies could enter a human [17]. Ten mollusk species from coastal cities along the Bohai Sea, China, were found to contain an average of 18.82 ng/g dry weight of NOR, range 0 - 370 ng/g dry weight [23]. Three mollusk species from Pearl River Delta had a mean NOR contamination of 31 ng/g wet weight, range 0 – 256 ng/g wet weight [24].

จุฬาลงกรณ์มหาวิทยาลัย
Chulalongkorn University

Table 3 List of NOR contaminations in the WWTP discharge and in the environment

Location	Notes	WWT method	Levels	Ref.
1. Patanchery Enviro Tech Ltd. WWTP, Patancheru, India	WWTP effluent	Oxygenated biological treatment	25 μg/l	[21]
2. Lake 1, Patancheru, India	Upstream of WWTP of pharmaceutical industry	Oxygenated biological treatment	60 – 520 μg/l	[21]
3. Lake 2, Patancheru, India	Upstream of WWTP of pharmaceutical industry	Oxygenated biological treatment	91– 200 μg/l	[21]
4. Groundwater well, Patancheru, India	Nearby village of WWTP	Oxygenated biological treatment	ND - 31 ng/l	[21]
5. Isakavagu-Nakkavagu River, Patancheru, India	Downstream of WWTP	Oxygenated biological treatment	ND – 4.7 μg/l	[21]
6. Machakos WWTP, Kenya	WWTP effluent	Stabilization pond	4.2 μg/l	[22]
7. Machakos WWTP, Kenya	Suspended particulate matter in WWTP effluent	Stabilization pond	82,267 μg/kg	[22]
8. Mitheu River, Machakos, Kenya	500 meters upstream of Machakos WWTP	-	0.6 - 1.6 μg/l	[22]
9. Mitheu River, Machakos, Kenya	500 meters downstream of Machakos WWTP	-	2.2 - 4.9 μg/l	[22]
10. Chao Phraya Abhaibhubejhr Hospital, Thailand	WWTP effluent	Activated sludge oxidation ditch	5.04 μg/l	[3]

Table 3 [Continued] List of NOR contaminations in the WWTP discharge and in the environment

Location	Notes	WWT method	Levels	Ref.
11. Bang Pakong Hospital, Thailand	WWTP effluent	Oxidation pond	2.53 μg/l	[3]
12. Pig farm, Thailand	Discharge water	NG	39.2 μg/l	[3]
13. Bang Pakong River, Thailand	15 collection points along the river	-	1.79 - 20.75 μg/l	[3]

Chulalongkorn University

2.2.2 Studied adverse effect of NOR in the environment

Some of the abovementioned levels of NOR contamination in the environment in Table 3 exceeded the PNEC-ENV (environmental predicted no-effect concentration) at 120 μg/l meaning that NOR can exist up to this particular concentration without adverse effect to the environment [25].

Examples of studied negative effects to the ecosystem and enironment are as followed. Firstly, trace levels of NOR in natural water was found to impact marine life. 0.1 mg/l of NOR can negatively alter the biochemicals in zebrafish, such as stimulating their glutathione peroxidase enzyme action [4].

NOR mixed in soil also inhibited that disemmination and degradation of several herbicides including simazine, atrazine, terbuthylazine, acetochlor, and metolachlor. When the contamination exceeded 5 mg/kg for 30 days, the half life of simazine increased from 16.1 days to 19.3 days, and the leftover simasize in soil increased from 24.2% to 30.4% [11].

A study on a freshwater plankton species, *Daphnia magna*, found that high NOR concentrations of significantly increased the mortality rate from 2% at 50 mg/l to 100% at 400 mg/l in 96 h compared to the control mortality rate. At sublethal levels, NOR concentrations of 25, 50, and 100 mg/l reduced average swimming ability by 22.1%, 44.3% and 61.5%, respectively, after 12 h of exposure. After 4-12 h of exposure to 25-100 mg/l NOR, feeding rate was also greatly affected [26].

จุฬาลงกรณ์มหาวิทยาลัย
Chulalongkorn University

2.2.3 Norfloxacin properties

Another common name for NOR is Noroxin. 2-D chemical structure of NOR and the 3-D version are presented in Fig. 3 and 4 respectively.

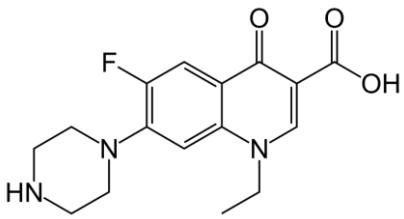

Figure 3 2-D chemical structure of NOR

(source: https://en.wikipedia.org/wiki/Norfloxacin)

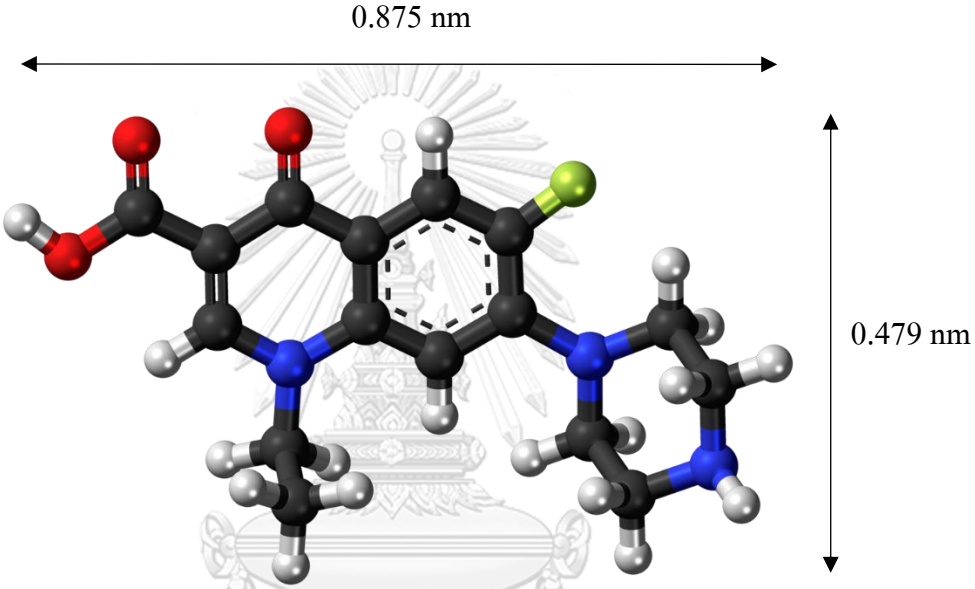

จุฬาลงกรณ์มหาวิทยาลัย
Chulalongkorn University

Figure 4 3-D chemical structure and dimension of NOR

(source: https://commons.wikimedia.org/wiki/File:Norfloxacin_molecule_ball.png)

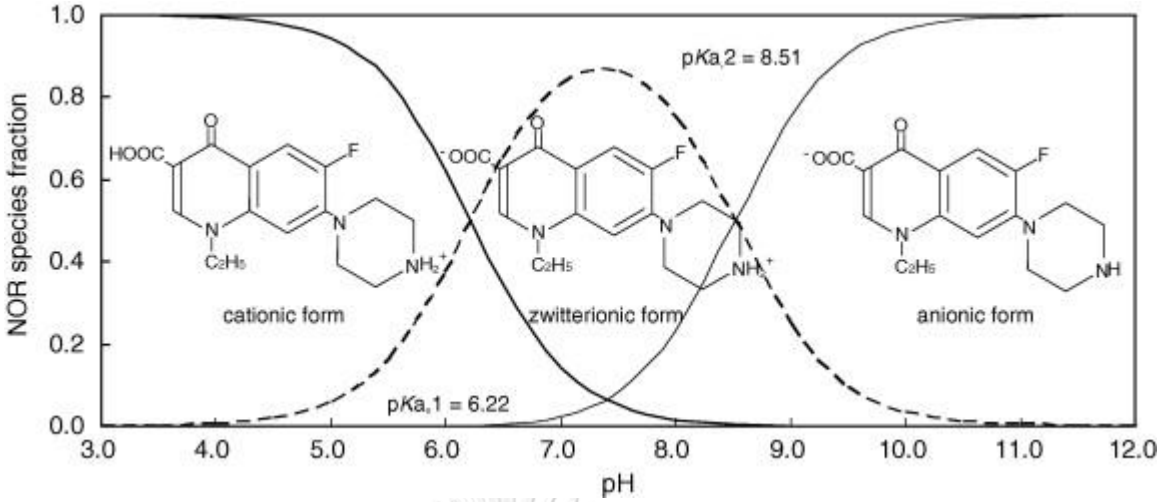

Figure 5 Molecular structure of NOR and its ionic forms as a function of pH [27]

NOR is a zwitterion meaning it exists in both cationic and anionic form depending on the solution pH. Fig. 5 depicts the form of NOR at pH 3 – 12. NOR undergoes two diassociation when dissolved in water: pK_{a1} = 6.22, and pK_{a2} = 8.51. Properties of NOR can be found in Table 4.

Table 4 NOR experimental properties [28]

Property Name	Property Value
Molecular weight	319.331
Melting point	227 °C
Water solubility	280 mg/l at 25 °C (pH dependent)
pKa	pK_{a1} = 6.22, pK_{a2} = 8.51

จุฬาลงกรณ์มหาวิทยาลัย CHULALONGKORN UNIVERSITY

2.3 Activated carbon

Activated carbon or activated charcoal is a carbon material that has porous structure and high surface area. Pores in activated carbon are of varying sized which can be categorized as micropores (<2 nm), mesopores (2-50 nm), and macropores (>50 nm) according to IUPAC. For

organic emerging pollutant adsorption, mesopores are the most desirable because they're larger than a lot of organic pollutant molecules while still providing higher surface area than macropores [2 9] . Additionally, mesopores facillitates the transportation of adsorbates to micropores from molecules that can fit inside micropores. Examples of organic pollutant compounds and their dimension are given in Table 5.

able 5 Structure and dimension of organic pollutant compounds [30]

Organic compounds	Structure	dimension (nm)
Phenol	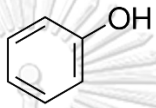	0.51 x 0.37 x 0.33
Aniline	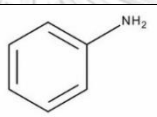	0.51 x 0.43 x 0.41
Methyl orange	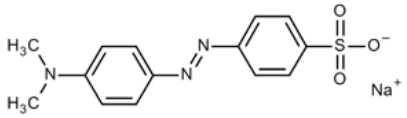	1.31 x 0.55 x 0.18
Methylene blue	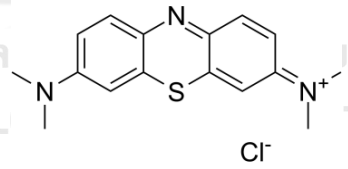	1.26 x 0.77 x 0.65
Rhodamine B	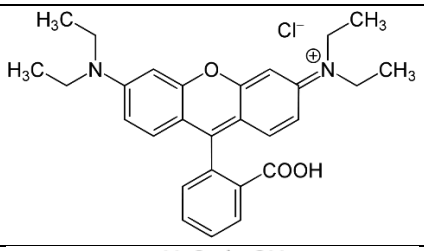	1.59 x 1.18 x 0.56
Victoria blue B	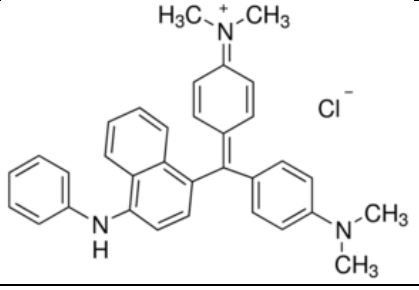	1.47 x 1.41 x 0.44

2.4 Biomass and agricultural waste

Biomass is a renewable organic material that comes from plants. Biomass consists of three main biopolymer compounds; cellulose, hemicellulose, and lignin, at different compositions. Carbon, oxygen, and hydrogen are the elements that are found in lignocellulosic structure. These lignocellulosic compounds play different roles in biomass. Cellulose is a straight chain biopolymer which is the main fiber making up cell walls of plant cells. Hemicellulose is a branch biopolymer works to straighten the cell walls by binding with cellulose. Lignin acts like a glue between fibers supporting the structure of the plant and adding rigidity. The structures of cellulose, hemicellulose, and lignin are displayed in Fig. 6 – 8 respectively.

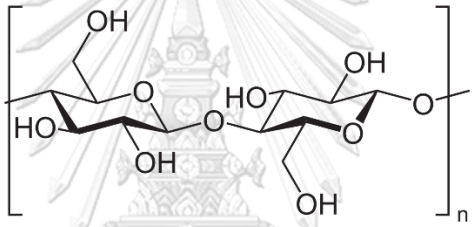

Figure 6 Structure of cellulose

[https://en.wikipedia.org/wiki/Cellulose]

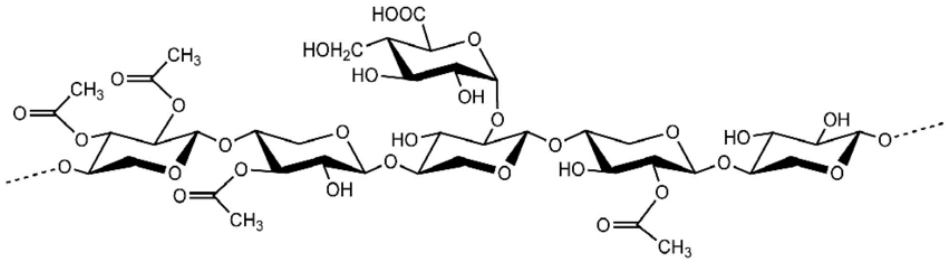
HOOC
HOH2C
HO
O
OH
CH3
O
CH3
O
O
O

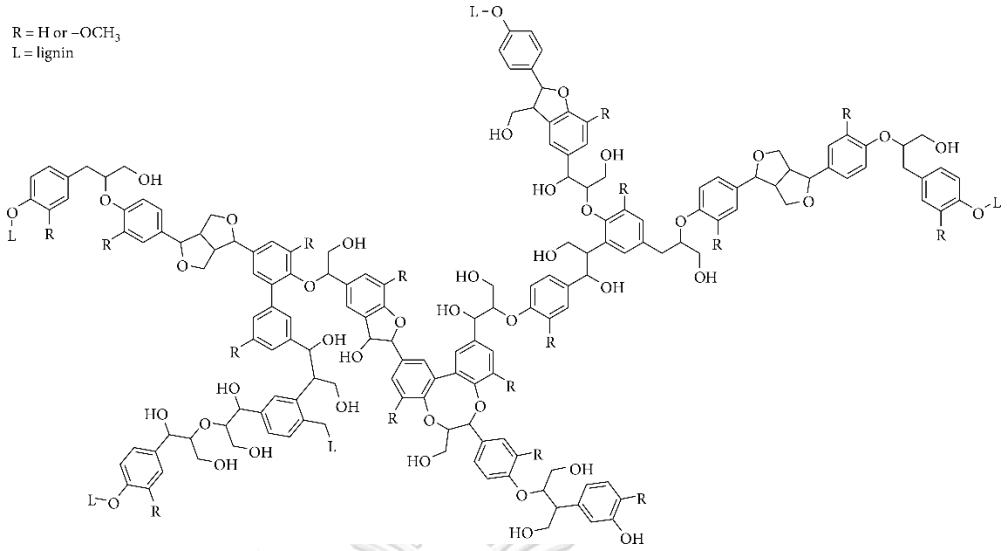

Figure 8 Structure of lignin [32]

2.5 Carbonization process

Carbonization process is the conversion of biomass to carbonaceous material by a heat treatment process called pyrolysis. During the process, biomass is heated under limited oxygen atmosphere and chemical bonds in cellulose, hemicellulose, and lignin decompose. Pyrolysis products include gas, tar (liquid), and char (solid) [33, 34].

2.6 Activation process

จุฬาลงกรณ์มหาวิทยาลัย
Chulalongkorn University

The char products from carbonization process still have low porosity and low adsorption capabilities. Activation process is where the porous properties are enhanced. There are two types of activation methods: chemical activation, and physical activation (thermal activation). Fig. 9 shows the steps of biomass conversion to activated carbon through chemical activation and physical activation.

2.6.1 Chemical activation

Chemical activation involves a presence of an activating agent, most commonly $ZnCl_2$, H_3PO_4, KOH, HCl, etc [35]. Each chemical has different mode of action and

affects porosity differently. The biomass can be carbonized and activated simultaneously in the same chamber in chemical activation. The ratio of chemical activating agent and activation temperature are also vital to the porous structure, pore distribution, surface area, and surface functionality of the activated carbon product [36].

2.6.2 Physical activation

Commercially, physical activation is a two-step process. The first step is carbonization in an inert atmosphere, such as N_2. The second step is the activation under oxidising atmosphere, such as steam, CO_2, or a mixture of CO_2, N_2 and air [35]. Physical activation typically requires higher temperature than chemical activation at 800 - 1,000 °C which leads to higher energy consumption as well.

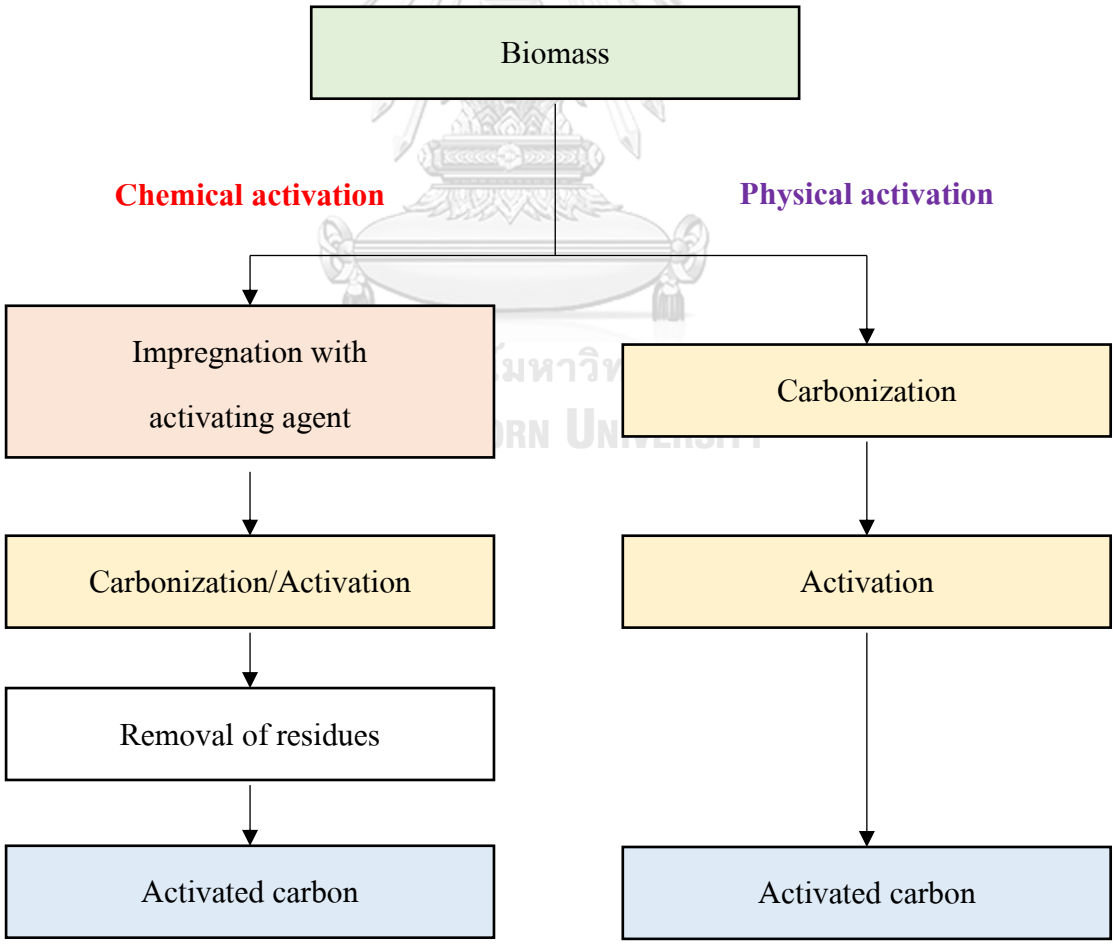

Figure 9 Activated carbon synthesis from biomass via chemical and physical activation flowchart

2.7 Adsorption

Adsorption is the adhesion of the adsorbate from a gas or liquid to the adsorbent surface. The adsorbate can be both organic and inorganic. Factors that affect adsorption include the surface area and porosity of the adsorbent, particle size, functional groups on the surface, temperature, pH of the solution, and concentration of the adsorbate, etc [37]. As illustrated in Fig. 10, adsorption process occurs in 4 steps as described in the following.

(1) Transportation of adsorbate molecules or ions from bulk solution to the boundary layer of the adsorbent. This step is rapid; therefore, it is not considered to be a rate-limiting step candidate.

(2) External diffusion of adsorbates from the boundary layer to the surface.

(3) Internal diffusion of adsorbates from the surface. (Intraparticle diffusion).

(4) Adsorption on active sites.

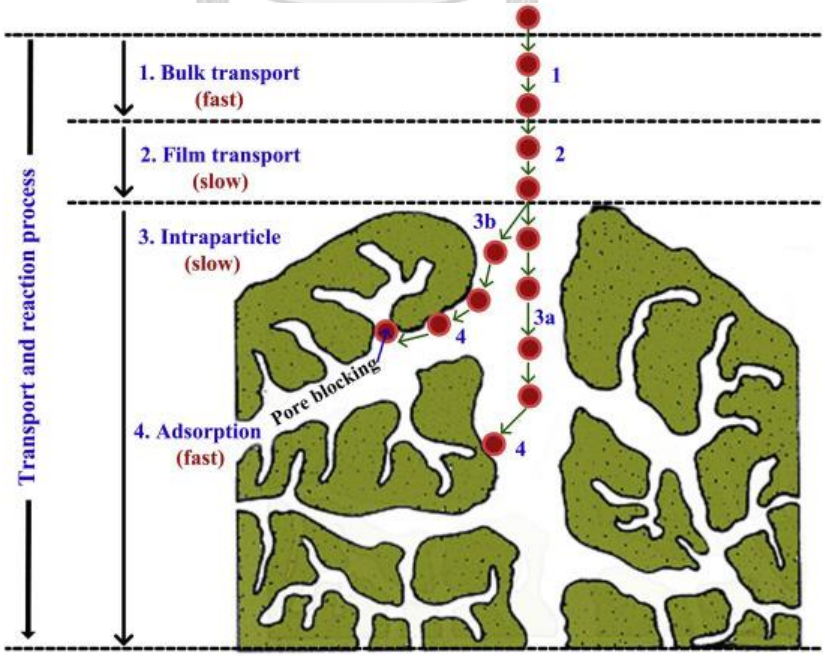

Figure 10 Transport processes during adsorption by a porous adsorbent [38]

2.7.1 Types of adsorption

2.7.1.1 Physical adsorption

This mode of adsorption is caused by physical forces. Since it's nonspecific, it could be a multi-layered process. Physical adsorption is weaker than chemical adsorption. The energy of physical adsorption is less than chemical adsorption.

2.7.1.2 Chemical adsorption

Chemical adsorption is caused by chemical bonding between the adsorbate and adsorbate and adsorbent. Though more selective than physical adsorption, it is far stronger. The energy of chemical adsorption is higher than physical adsorption. Surface functionality greatly affects chemical adsorption. Since the adsorption occurs at specific adsorption sites at the surface, it's a monolayer process.

In the quantitative part of adsorption experiment, the removal percentage and adsorbate uptake per mass of adsorbent are essential. The removal percentage (%removal) and norfloxacin (NOR) uptake at equilibrium (q_e) are calculated by eq (1) and (2):

จุฬาลงกรณ์มหาวิทยาลัย
CHULALONGKORN UNIVERSITY

$$\%\text{removal} = \left(\frac{C_0 - C_e}{C_0}\right) \times 100 \quad (1)$$

$$q_e = \frac{(C_0 - C_e)V}{W} \quad (2)$$

where %removal is NOR removal percentage,

q_e is the NOR uptake at equilibrium (mg/g),

C_0 is the initial concentration of adsorbate (mg/l),

C_e is the equilibrium concentration of adsorbate (mg/l),

V is the volume of the solution (l),

W is the mass of the adsorbent (mg).

2.8 Adsorption isotherm models

Adsorption isotherms provide information on the mechanism of adsorption and behaviour of adsorbate is solid and liquid system. In this work, 3 common isotherm models were selected: Langmuir, Freundlich, and D-R [39, 40].

2.8.1 Langmuir isotherm model

Langmuir model assumes that (1) the adsorption is a monolayer adsorption on homogeneous surface; (2) there is no interaction between adsorbate molecules; (3) each site can only hold one molecule; (4) heat of adsorption is constant. Non-linear Langmuir model is written in eq (3) [41].

$$q_e = \frac{q_m K_L C_e}{1+K_L C_e} \quad (3)$$

where q_e is the NOR uptake at equilibrium (mg/g),

K_L is the Langmuir isotherm constant (l/mg) relating to energy of adsorption,

C_e is the equilibrium concentration of adsorbate (mg/l),

q_m is the maximum monolayer adsorption capacity (mg/g).

จุฬาลงกรณ์มหาวิทยาลัย
Chulalongkorn University

Furthermore, Langmuir isotherm can be expressed as a dimensionless term R_L shown in eq (4).

$$R_L = \frac{1}{1+K_L C_0} \quad (4)$$

where R_L is the Langmuir separation factor,

K_L is the Langmuir isotherm constant (l/mg),

C_0 is the initial concentration of NOR (mg/l).

R_L describes the shape of the isotherms to be either favourable ($R_L < 1$), linear ($R_L = 1$), or unfavourable ($R_L > 1$).

2.8.2 Freundlich isotherm model

Freundlich isotherm model is an empirical model which assumes that (1) the adsorption is a multilayer adsorption on heterogeneous surface; (2) adsorbate molecules interact with one another; (3) heat of adsorption is not constant. Non-linear Freundlich model is written in eq (5).

$$q_e = K_F C_e^{1/n} \quad (5)$$

where K_F is the Freundlich constant $(mg/g)(1/mg)^{1/n}$,

n is a dimensionless term regarding the magnitude of surface heterogeneity. If n > 1, the adsorption is favourable.

2.8.3 Dubinin-Radushkevitch (D-R) isotherm model

D-R model is a temperature-dependent semiempirical model often used to express adsorption mechanism with Gaussian energy distribution onto a heterogeneous surface [42]. D-R isotherm is expressed as follows in eq (6 – 8) [39]:

$$q_e = q_{DR} e^{-K_{RD}\varepsilon^2} \quad (6)$$

$$\varepsilon = RT\ln\left(1 + \frac{1}{C_e}\right) \quad (7)$$

$$E = \frac{1}{\sqrt{2K_{DR}}} \quad (8)$$

จุฬาลงกรณ์มหาวิทยาลัย
CHULALONGKORN UNIVERSITY

where q_{DR} is the D-R adsorption capacity (mg/g),

K_{DR} is a constant related to the adsorption energy (mol^2/kJ^2),

ε is the Polanyi potential,

R is the gas constant (J/mol·K),

T is the absolute temperature (K),

E is the free energy of adsorption per molecule of adsorbate (kJ/mol). E value can distinguish the adsorption mechanism. E < 8 kJ/mol is physical adsorption, 8 kJ/mol < E < 16 kJ/mol is chemical adsorption, E > 16 kJ/mol is ion exchange.

2.9 Adsorption kinetics models

Adsorption kinetics refers to the study of rate of adsorbate uptake by the activated carbon. Kinetic models give information about adsorption pathways and probable adsorption mechanism. 4 adsorption kinetics models are employed: Pseudo first order model, Pseudo second order model, Elovich model, and Intra-particle diffusion model [39, 43].

The adsorbate uptake at a given time is calculated by eq (9).

$$q_t = \frac{(C_0 - C_t)V}{W} \quad (9)$$

where q_t is the amount of NOR uptake at a given time t (mg/g),

C_0 is the initial concentration of adsorbate (mg/l),

C_t is the remaining concentration of adsorbate at time t (mg/l),

V is the volume of the solution (l),

W is the dry mass of the adsorbent (mg).

2.9.1 Pseudo first order model (PFO)

PFO model is one of the most common models. The Lagergren differential form is shown in eq (10). The integrated non-linear form is written in eq (11). Experiments that PFO describes usually have high initial concentration of adsorbate allowing for quick adsorption.

$$\frac{dq_t}{dt} = k_1(q_{e1} - q_t) \quad (10)$$

$$q_t = q_{e1}[1 - \exp(-k_1 t)] \quad (11)$$

where k_1 is the PFO rate constant (1/min),

q_t is the amount of NOR uptake at a given time t (mg/g),

t is the elapsed time (min),

q_{e1} is the amount of NOR adsorbed at equilibrium according to the PFO model (mg/g).

2.9.2 Pseudo second order model (PSO)

The differential equation for PSO and the integrated non-linear form are written in eq (10) and (11), respectively.

$$\frac{dq_t}{dt} = k_2(q_{e2} - q_t)^2 \quad (12)$$

$$q_t = \frac{k_2 q_{e2}^2 t}{1 + k_2 q_{e2} t} \quad (13)$$

where k_2 is the PSO rate constant (g/mg·min),

q_{e2} is the amount of NOR adsorbed at equilibrium according to the PSO model (mg/g).

The initial adsorption rate is given by h in eq (14), calculated by k_2 and q_{e2} obtained from the PSO model.

จุฬาลงกรณ์มหาวิทยาลัย
CHULALONGKORN UNIVERSITY

$$h = k_2 q_{e2}^2 \quad (14)$$

where h is the initial rate of adsorption (mg/g·min).

2.9.3 Elovich model

Elovich model describes multilayer adsorption on heterogeneous surface based on a kinetic principle that rate of adsorption decreases exponentially with the increase in adsorbate uptake [44]. Elovich model is written in eq (15-16).

$$\frac{dq_t}{dt} = \alpha \exp(-\beta q_t) \quad (15)$$

$$q_t = \frac{1}{\beta} \ln(1 + \alpha\beta t) \quad (16)$$

where α is the initial adsorption rate (mg/g·min),

β is the desorption constant (g/mg).

2.9.4 Intra-particle diffusion model (IPD)

The linear IPD model equation is written in eq (17) [45]. Proposed by Weber and Morris, when the regression of eq (17) passes through the origin, intra-particle diffusion is the rate-limiting step.

$$q_t = k_i t^{0.5} + C_i \tag{17}$$

where k_i is the IPD constant (mg/g·min$^{1/2}$),

Ci is the y-intercept of the regression and IPD constant associated with the film thickness. (mg/g).

2.10 Adsorption thermodynamics

Thermodynamics can give important information about spontaneity and energy of adsorption. Van't Hoff equation, eq (18), connects the change of equilibrium constant (K_c) to the change of temperature. K_c is calculated from K_L in Langmuir isotherm model through eq (19). ΔG is calculated by eq (20).

$$\ln(K_C) = \frac{\Delta S}{R} - \frac{\Delta H}{RT} \tag{18}$$

$$K_C = K_L \times MW_A \times 55.5 \times 1000 \tag{19}$$

$$\Delta G = \Delta H - T\Delta S \tag{20}$$

where Kc is the equilibrium constant,

R is the gas constant, 8.314 J/mol·K,

T is the temperature (K),

ΔG is the change in Gibb's free energy (kJ/mol),

ΔH is the enthalpy change (kJ/mol),

ΔS is the entropy change (J/mol·K),

K_L is the Langmuir isotherm constant (l/mg) relating to energy of adsorption,

MW_A is the molecular weight of adsorbate (g/mol).

2.11 Activated carbon from turmeric waste

Several activated carbons were created from industrial turmeric waste from Erode City, Tamil Nadu, India, through chemical activation at 800 °C. The activating agents include HCl, H_2SO_4, $ZnCl_2$, Na_2SO_4, Na_2CO_3, $CaCO_3$, $CaCl_2$, H_2SO_4+$NH_4S_2O_8$, H_2SO_4+H_2O_2, resulting in activated carbon with surface area 790, 361, 1350, 352, 291 ,221, 1264, 898, 703 m^2/g, and Iodine number 755, 342, 1265, 332, 282, 212, 1210, 839, 676 mg/g, respectively. The carbon that was activated by $CaCl_2$ was then used to adsorbed direct orange dye (anionic), acid blue 40 (anionic), basic red (anionic), and Cibacron brilliant yellow (cationic), the removal efficiencies were 55%, 86%, 30%, และ 51% respectively [46].

Another turmeric waste activated carbon study was also from Erode, India. Activated carbon generated from turmeric waste in a previous study, particle size 106.25 μm, was packed into a fixed bed column to remove acid blue 25 dye. The column's inner diameter was 3.35 mm. It was found that the adsorption efficiency within initial dye concentration range 20 – 60 mg/l was 60.9 – 90.8% with 38 – 115 retention time. It was concluded that turmeric waste activated carbon can remove dye from wastewater [47].

จุฬาลงกรณ์มหาวิทยาลัย
Chulalongkorn University

2.12 Norfloxacin adsorption

Other works regarding NOR adsorption are compiled in Table 6, categorized into 4 groups as follows: carbon nanotube, synthetic material, biomass-based material, and commercial activated carbons. For example, activated carbon from Fisher Scientific showed the higher NOR adsorption capacity than three carbon nanotubes: carboxylated carbon nanotube, graphitized carbon nanotubes, hydroxylated carbon nanotubes, because of activated carbon's high surface area (664 m^2/g) [48].

From group 3 biomass-based, cauliflower roots were used as the precursor to synthesize biochar via carbonization in a muffle furnace under limited oxygen atmosphere at 500 °C for 6 hours. The obtained biochar had total pore volume, micropore volume, and mesopore volume of 0.15, 0.07, and 0.08 cm^3/g respectively. S_{BET} was 232.15 m^2/g. The cauliflower root biochar was used to adsorb NOR to study adsorption isotherms, kinetics, and thermodynamics. The Langmuir maximum monolayer adsorption capacity (q_m) was 29.50 mg/g [19].

Activated magnetic biochars (AMB) were derived from corn stalks (CAMB), reed stalks (RAMB), and willow branches (WAMB) by simultaneous carbonization, magnetization, and activation. They had a large specific surface area (> 700 m^2/g) and pore volume (> 0.3 cm^3/g). Corn activated magnetic biochar had the highest NOR adsorption capacity out of the three adsorbents (CAMB, RAMB, WAMB) at 7.247 mg/g despite not having the highest porosity [49].

Another group of excellent NOR adsorbent is synthetic materials. Commercial hypercrosslinked resin (MN-202), aminated polystyrene resin (MN-150), and macroporous resin (XAD-4) were used to adsorb NOR. The resin MN-202 and MN-150 had a mixed pore structure with considerable amount of mesopores. Their NOR adsorption capacities were MN-202 > MN-150 > XAD-4. It was likely that the adsorption mechanism for XAD-4 was hydrophobic effect while MN-202 and MN-150 mechanism was pore filling with the help of hydrophobic effect, electrostatic interaction, H-bond and π–π electron interactions [50].

จุฬาลงกรณ์มหาวิทยาลัย
Chulalongkorn University

Table 6 List of other adsorbents in literature and their NOR adsorption capacities

Adsorbent	**S_{BET} (m^2/g)**	**Pore volume (cm^3/g)**	**Pore size (nm)**	**Q_m (mg/g)**	**Ref**
Group 1 Carbon nanotubes					
1. Carboxylated multiwall carbon nanotube	160	-	0.564	88.50	[50]
2. Graphitized carbon nanotubes	117	-	-	57.55	[48]
3. Carboxylated carbon nanotubes	164	-	-	54.44	[48]
4. Hydroxylated carbon nanotubes	228	-	-	76.34	[48]
Group 2 Synthetic materials					
5. Hyper-crosslinked resin	1160	-	5.19	185.2	[50]
6. Aminated polystyrene resin	815	-	5.45	149.3	[50]
7. Macroporous resin	880	-	5.80	153.8	[50]
8. Iron-doped activated alumina (Al_2O_3/Fe)	141	-	-	32.55	[51]
9. Fe-MCM-41 molecular sieves	961	V_T = 0.90	3.75	102.9	[52]
Group 3 Biomass-based materials					
10. Pomelo peel-based biochar	1.71	V_T = 0.003	5.90	34.88	[53]
11. Cauliflower roots biochar	232	V_T = 0.15 V_{mic} = 0.07 V_{meso} = 0.08	-	31.15	[19]
12. Cassava waste KOH-modified biochar	128	V_T= 0.010	2.42	1.960	[54]
13. Corn activated magnetic biochar	761	V_T = 0.37	-	7.247	[49]
14. Reed activated magnetic biochar	778	V_T = 0.33	-	3.514	[49]
15. Willow activated magnetic biochar	857	V_T = 0.40	-	6.259	[49]
16. Hematite-reed straw biochar composites	135	V_T = 0.086	2.54	4.074	[55]
17. Pyrite-reed straw biochar composites	54.5	V_T = 0.053	3.90	5.106	[55]
18. Granular activated carbon from maize straw	1200	V_T = 1.31 V_{mic} = 0.13	-	112.8	[56]
19. Biochar derived from *luffa* sponge	822	-	5.35	278.0	[57]

จุฬาลงกรณ์มหาวิทยาลัย
CHULALONGKORN UNIVERSITY

Table 6 [continued] List of other adsorbents in literature and their NOR adsorption capacities

Adsorbent	**S_{BET} (m^2/g)**	**Pore volume (cm^3/g)**	**Pore size (nm)**	**Q_m (mg/g)**	**Ref**
Group 4 Commerical activated carbons					
20. Commercial activated carbon from wood charcoal (Fisher Scientific)	664	-	-	112.5	[48]
21. Commercial powder activated carbon (mesh 200 ground Filtrasorb-400, Calgon Corp., USA)	-	-	-	237	[58]

จุฬาลงกรณ์มหาวิทยาลัย
CHULALONGKORN UNIVERSITY

Chapter 3

Methodology

3.1 Materials

3.1.1 Turmeric waste (TW)

TW came from the rhizome of turmeric plant that had been through curcumin extraction process in a Thai herbal medicine manufacturing factory. The process is shown in Fig. 11.

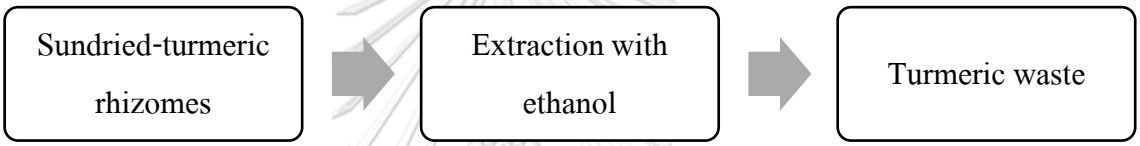

Figure 11 Turmeric waste process

3.1.2 Chemicals

All the chemicals used in this research are written in Table 7.

Table 7 Chemicals involved in this research and details

จุฬาลงกรณ์มหาวิทยาลัย
Chulalongkorn University

Chemical	State	Formula	MW	Grade	Manufacturer
Nitrogen	Gaseous	N_2	28.01	99.99% purity	Thai industrial gas (TIG)
Calcium chloride	Solid	$CaCl_2$	110.98	Analytical grade	Carlo Erba
Hydrochloric acid	Liquid	HCl	36.458	Grade AR	QReC
Norfloxacin	Solid	$C_{16}H_{18}FN_3O_3$	319.33	TLC grade	Sigma-Aldrich

3.1.3 Furnace

The furnace consists of two main components as illustrated in Fig. 12. Firstly, the nitrogen source is a gas cylinder contacted to the lid of the chamber. During the carbonization process, nitrogen was fed into the chamber at a constant rate from the top. The second part is the chamber where the turmeric waste was placed at the bottom without a crucible. The thermocouple was inserted to measure and control the temperature inside the chamber. The gas/liq outlet was at the top of the chamber.

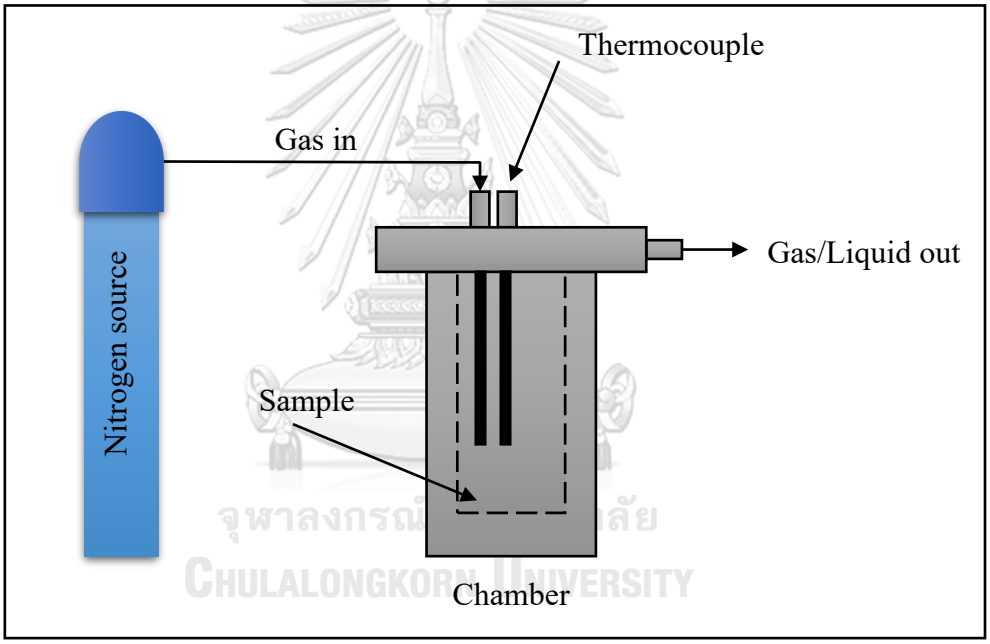

Figure 12 Schematic diagram of the furnace

3.1.4 Analytical instruments

1. Thermogravimetric analysis (TGA, Q50 V6.7 Build 203, TA instruments)

2. Field-emission electron scanning microscope and energy dispersive X-ray spectrometer (FE-SEM/EDX, Hitachi, SU3500)

3. Fourier transform infrared spectrophotometer (FTIR, Thermo scientific, NICOELT iZ10)

4. Nitrogen adsorption-desorption apparatus (Autosorb MP, QuantaChrome)

5. X-ray diffractometer (Rigaku, Smartlab, XRD)

6. Raman microscope (Horiba, XploRA PLUS)

7. UV-Visible spectrophotometer (UV-Vis, Hach, DR6000)

3.2 Methodology

3.2.1 Turmeric waste pretreatment

The collected turmeric waste (soaked with ethanol) from the extraction process was air-dried at room temperature and placed in an electric oven at 80°C, 24 h to remove moisture and alcohol.

จุฬาลงกรณ์มหาวิทยาลัย
CHULALONGKORN UNIVERSITY

3.2.2 Calcium chloride impregnation

The dried turmeric waste was sifted through a mesh 20 (0.841 mm) standard sieve and the coarse grain larger than mesh 20 was collected. Any lumps in the turmeric waste that had formed during storage was also removed. In a single batch preparation, 50 g of the dried turmeric waste was submerged in 500 g of 10%w/w of $CaCl_2$ solution (ratio $CaCl_2$: turmeric waste = 1:1) for 24 h at room temperature. After 24 h, the liquid was drained and the turmeric waste was dried in the oven at 80°C for 24 h.

$CaCl_2$ was chosen as the chemical activator for turmeric waste activated carbon because it resulted in the second highest surface area (1,264 m^2/g), second to $ZnCl_2$ (1,350 m^2/g), in research by Karthikeyan, Sivakumar, and Palanisamy, whether the enormous surface area was from micropores or mesopores was not discussed. It was suggested that $CaCl_2$ and $ZnCl_2$ had such good surface area results due to the effectiveness of the removal of organic matter [46]. $CaCl_2$ is considered more environmentally friendly than $ZnCl_2$, so it was chosen.

3.2.3 Turmeric waste activated carbon synthesis

In a batch of carbonization, 50 g of the $CaCl_2$ impregnated turmeric waste was put into a cylindrical chamber. The carbonization and activated step occurred simultaneously under N_2 atmosphere, flow rate 100 cm^3/min. The temperature ramp was fixed at 10°C/min, once the temperature reached the carbonization temperature, it was held for 2 h. The independent variable in this carbonization step is the carbonization temperature 500 – 900 °C.

3.2.4 Acid washing

The synthesized activated carbons were then washed in 0.10M HCl and deionized water until pH reached neutral to remove calcium in the pore structure.

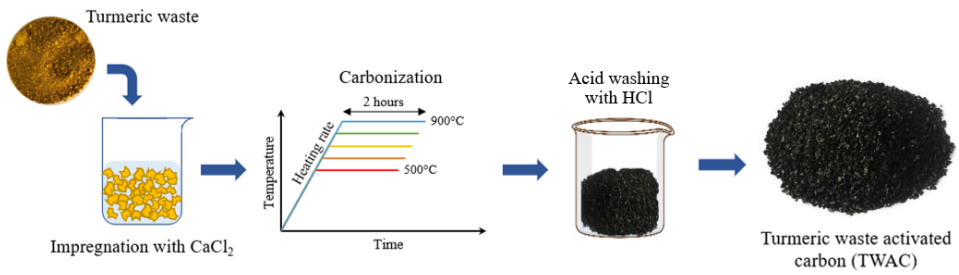

Figure 13 Preparation of turmeric waste activated carbon

Fig. 13 shows the schematic representation of turmeric waste activated carbon synthesis.

3.2.5 Turmeric waste biochar synthesis

The dried turmeric waste without $CaCl_2$ impregnation was also carbonized to show the effect of $CaCl_2$ impregnation on the carbons. 50 g of the dried turmeric waste was put into a cylindrical chamber. The carbonization took place under N_2 atmosphere, flow rate 100 cm^3/min. The temperature ramp was fixed at 10°C/min, once the temperature reached 700 °C, it was held for 2 hours.

The assigned abbreviated names for all the synthesized activated carbon and biochar are given in Table 8.

Table 8 Synthesis conditions of the prepared activated carbon and biochar from turmeric waste

Samples	**Conditions**		
	Activated agent	**Process**	**Temperature**
TWB700	-	Carbonization with N_2	700 °C
TWAC500	$CaCl_2$	Carbonization with N_2 and chemical activation	500 °C
TWAC600	$CaCl_2$	Carbonization with N_2 and chemical activation	600 °C
TWAC700	$CaCl_2$	Carbonization with N_2 and chemical activation	700 °C
TWAC800	$CaCl_2$	Carbonization with N_2 and chemical activation	800 °C
TWAC900	$CaCl_2$	Carbonization with N_2 and chemical activation	900 °C

จุฬาลงกรณ์มหาวิทยาลัย
Chulalongkorn University

3.3 Characterization of turmeric waste and turmeric waste activated carbon (TWAC)

3.3.1 Thermogravimetric analysis

The thermal stability of turmeric waste (TW) and $CaCl_2$ impregnated turmeric waste (TW-$CaCl_2$) was studied on thermogravimetric analysis instruments in the temperature range of 30-900°C under N_2 atmosphere, ramp 10.00 °C/min to 900.00 °C. The data was reported in 2 terms, weight% (%) and derivative weight (%/°C)

3.3.2 Field-emission electron scanning microscope and energy dispersive X-ray spectrometer

FE-SEM was used to study the surface morphology and texture of the synthesized activated carbon. The microscopic images were taken at 60x and 5,000x magnifications. EDX was also applied to TWAC700 to determine the chemical composition in 3 areas of the sample to verify the carbon material and discover the residue inside the carbon.

3.3.3 Nitrogen adsorption-desorption apparatus

Nitrogen adsorption-desorption apparatus was used to find the N_2 adsorption-desorption isotherm at 77 K of TWAC500 – 900 and TWB700. From the adsorption data, the Brunauer-Emmett-Teller (BET) and Dubinin-Radushkevich (D-R) models were used to estimate the specific surface area (S_{BET}) and micropore volume (V_{mic}), respectively. The average pore diameter was obtained by the Gurwitch rule. From the desorption data, the Barrett-Joyner-Halenda (BJH) method was used to estimate the mesopore volume (V_{meso}) and pore size distribution. The operating conditions for the degassing step are 150 °C, and 24 h.

จุฬาลงกรณ์มหาวิทยาลัย
CHULALONGKORN UNIVERSITY

3.3.4 X-ray diffractometer

X-ray diffraction analysis was done on TWAC500 – 900. X-ray diffraction is used to analyse the crystalline structure of the sample which can be both quantitative and qualitative. XRD is also commonly used for phase identification. In this work, all patterns were measured at 2θ in a range of 10-80 degrees by a 30kV diffractometer equipped with a fixed monochromator

and a Cu Kα radiation source which was set an accelerating voltage of 40 kV, an applied current of 30 mA and a scan speed of 5 θ/m.

3.3.5 Raman spectroscopy

Raman spectroscopy analysed TWAC500 – 900 in this work. It is a light scattering chemical analysis technique. It is sensitive to the slight change in carbon material. In this research, Raman microscope equipped with a spectrophotometer was used to study the degree of graphitization and defects within the carbon structure. The conditions include excitation laser wavelength 532 nm and slit 200 μm.

3.3.6 Fourier transform infrared spectrophotometer

FTIR spectroscopy analysed the activated carbon that is chosen for NOR adsorption to study the surface functionality. The technique used in this study was ATR (attenuated total reflection).

Fig. 14 summarizes the turmeric waste activated carbon and biochar synthesis from the raw material to characterizations.

จุฬาลงกรณ์มหาวิทยาลัย
CHULALONGKORN UNIVERSITY

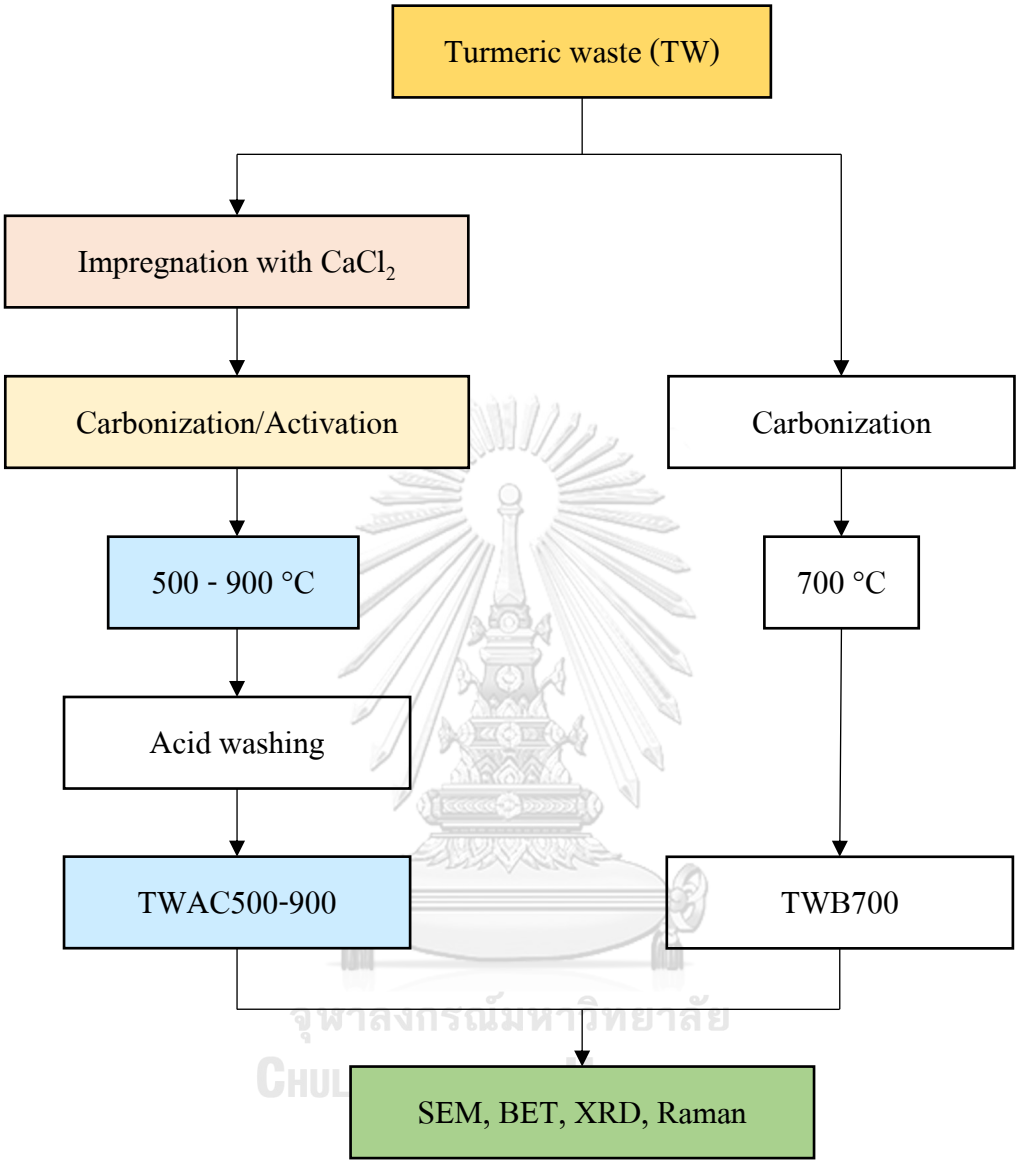

Figure 14 Flowchart of TWAC500-900 synthesis and characterization

3.4 Norfloxacin adsorption

Norfloxacin (NOR) adsorption was conducted in batches. Turmeric waste activated carbon (TWAC) was mixed in NOR solution and shaken at 200 rpm. The incubator shaker kept a constant temperature throughout the experiments. After a given time for each experiment, the carbon was removed from the flasks by a 0.45 μm Nylon syringe filter, and the clear solution was analysed by UV-vis spectrophotometer to find the final concentration.

3.4.1 UV-vis spectrophotometer

As stated by Beer and Lambert's law, when a monochromatic light travels through a homogeneous medium, the concentration of the solution is directly proportional to its absorption of light [59]. In this study, the absorbance of NOR solution between 1 – 10 mg/l at maximum absorbance wavelength 277 nm was directly proportional to the concentration. Thus, the initial and final NOR concentrations were converted from the absorbance data at 277 nm and the absorbance/concentration calibration graph in the Appendix. Any other concentrations higher than 10 mg/l was diluted before measurement.

Norfloxacin adsorption study was divided into 5 sections as the following.

3.4.2 Effect of carbon dosage

จุฬาลงกรณ์มหาวิทยาลัย
Chulalongkorn University

Turmeric waste activated carbon range 0.25 – 3 g/l was used to adsorb NOR initial concentration 10 mg/l, pH 7, at 25 °C for 24 h. The aim was to determine the carbon dosage to be used in the next adsorption experiments.

3.4.3 Effect of initial concentration

1 g/l of turmeric waste activated carbon was used to adsorb NOR initial concentration 10 – 200 mg/l, pH 7, at 25 °C for 24 h.

3.4.4 Adsorption equilibrium

1 g/l of turmeric waste activated carbon was used to adsorb NOR initial concentration 5 – 200 mg/l, pH 7, at 25 °C for 24 h. The data obtained from this section was fitted with the adsorption isotherm models; Langmuir, Freundlich, and D-R by nonlinear regression.

3.4.5 Adsorption kinetics

1 g/l of turmeric waste activated carbon was used to adsorb NOR initial concentration 40 mg/l, pH 7, at 25 °C for 0 - 72 h. The data obtained from this section was fitted with the adsorption kinetics models; PFO, PSO, Elovich, and IPD by nonlinear regression.

3.4.6 Thermodynamics of adsorption

1 g/l of turmeric waste activated carbon was used to adsorb NOR initial concentration 20 - 80 mg/l, pH 7, at 20 - 40 °C for 24 h.

จุฬาลงกรณ์มหาวิทยาลัย
Chulalongkorn University

Chapter 4

Results and discussion

4.1 Characteristic of turmeric waste

4.1.1 Thermal stability of turmeric waste and calcium chloride impregnated turmeric waste

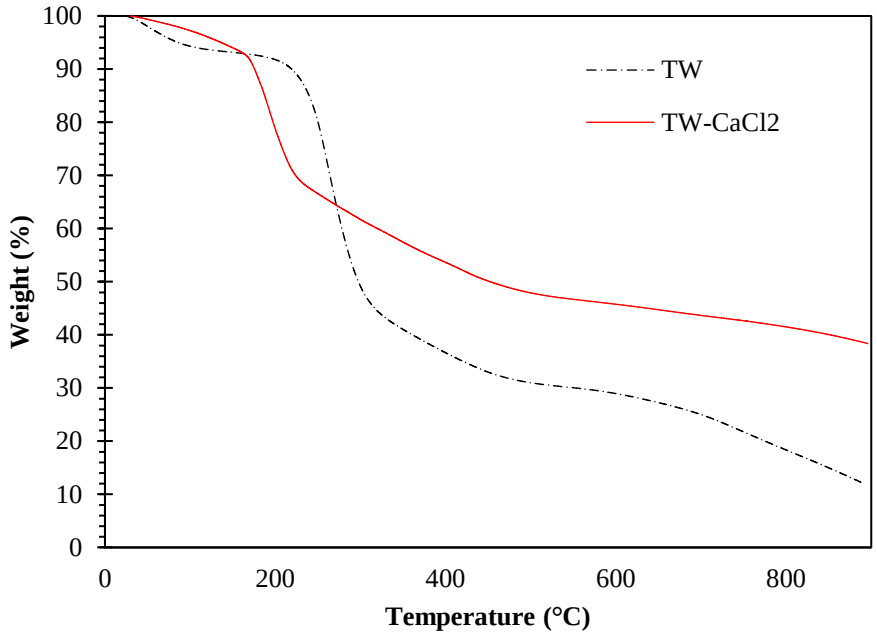

CHULALONGKORN UNIVERSITY

Figure 15 Thermogravimetric analysis (TGA) of turmeric waste (TW) and $CaCl_2$ impregnated turmeric waste (TW-$CaCl_2$)

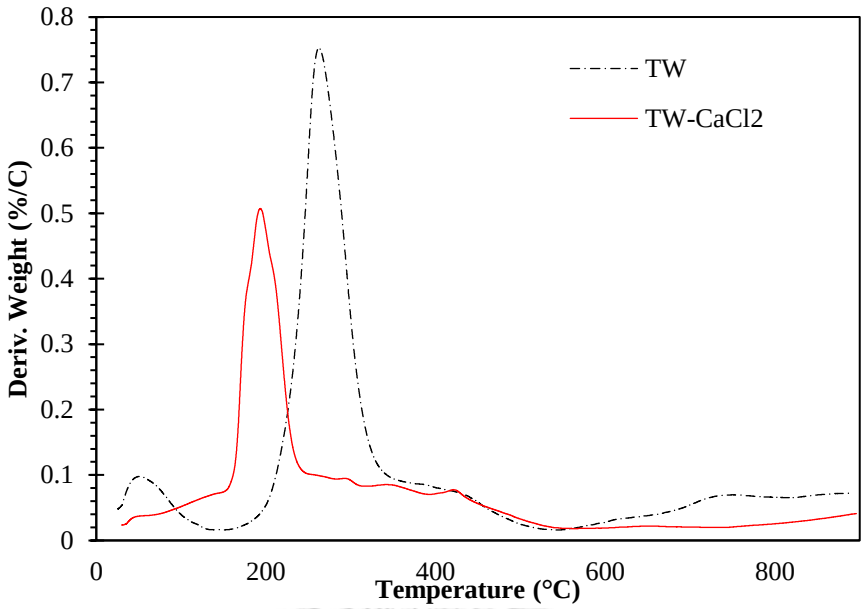

Figure 16 Derivative thermogravimetry (DTG) of TW and TW-$CaCl_2$

Fig. 15-16 shows the thermal stability of turmeric waste (TW) and $CaCl_2$ impregnated turmeric waste ($CaCl_2$-TW). For turmeric waste, the weight loss occurred in three prominent stages. The first stage on increasing the temperature from 25 °C to 150 °C, 7% of weight was lost due to evaporation of moisture, with the highest rate of loss at 50 °C. The second stage after the plateau at 150 °C to 540 °C had the largest weight loss at 62% of the sample, with the highest rate of decomposition at 260 °C which was the degradation of cellulose and hemicellulose. The last stage happened gradually due to lignin degradation until the temperature reached 900 °C [60]. The char residue was about 12%.

For TW-$CaCl_2$, the thermolysis occurred in two stages forgoing the first moisture evaporation stage. The temperature of the maximum rate of weight loss (T_M) lowered from 260 °C in pure turmeric waste to 200 °C. The second stage started at roughly the same temperature as the previous stage which is 540 °C. The char residue was 38%, the added weight partly came from the presence of calcium compounds in the sample.

From comparison of the mentioned stability results, $CaCl_2$ can lower degradation temperature of the turmeric waste's lignocellulosic structure. Dehydrating agents like $CaCl_2$ are

used in chemical activation as activating agent. Further, Ca^{2+} from $CaCl_2$ can interact with oxygens weakening hydrogen bonds during pyrolysis process which makes the hydroxyl groups and glycosidic bonds in lignocellulosic materials unstable. At elevated temperature, $CaCl_2$ also serves as a dehydration reaction catalyst [61, 62].

4.2 Turmeric waste activated carbon synthesis

4.2.1 N_2 adsorption-desorption isotherms and porosity of turmeric waste activated carbon

The N_2 adsorption-desorption isotherms for TWAC500 - 900 are illustrated in Fig. 17. According to IUPAC classification, the isotherms can be defined as type I and IV. The type I isotherm is characteristic of purely microporous material. The type IV, which often occurs in the same adsorbent with type I, is related to the presence of mesopores in the structure. Hysteresis loop is characteristic of type IV isotherm. TWAC500-900 all showed hysteresis loop type H3 which indicated that the pores are parallel pores. A summary of the type of adsorption and hysteresis loop is written in Table 9.

The effect of carbonization temperatures on BET surface area (S_{BET}), micropore volume (V_{mic}), mesopore volume (V_{meso}), and pore width (nm) is also shown in Table 9. As the carbonization temperature increased from 500 - 700 °C, the S_{BET} and pore volume increased from more degradation of volatile matter in this range. At 500 - 600 °C, the degradation of biomass was not complete because the temperature was too low therefore giving insufficient heat to the reaction. Higher temperature meant higher rate of pyrolysis which removed carbon atoms from the char resulting in an increase in the porous properties [60]. TWAC700 had the most developed pores with highest specific surface area, micropore volume, and mesopore volume at 334 m^2/g, 0.0954 cm^3/g, and 0.362 cm^3/g, respectively.

After the peak porosity of TWAC700, the sharp decrease of micropore and mesopore volume between TWAC700 and TWAC800 was because excess rate of carbonization at 800 °C could cause pore walls to collapse. Micropores could coalesce to form mesopores while mesopore walls collapsed to form macropores. This unwanted phenomenon is called pore sintering effect

where several smaller pores merge forming a large pore which caused surface area and pore volume to reduce [63].

The N_2 adsorption-desorption isotherms for TWB700 is illustrated in Fig. 17 as a comparison to TWAC500 – 900. According to IUPAC classification, the isotherm can be defined as type VI referring to nonporous material. A phenomenon called layering can be observed which is when isotherm shows a step like shape. The BET surface area (S_{BET}), micropore volume (V_{mic}), and pore width (nm) of TWB700 is also shown in Table 9. It can be concluded that TWAC500 – 900 had significantly better porous properties than TWB700, which was carbonized without the presence of $CaCl_2$, confirming that $CaCl_2$ was an effective chemical activating agent for turmeric waste.

Table 9 Porosity and isotherm characteristics of TWB and TWAC500-900

Sample	Porosity						
	Isotherm type	**Hysteresis loop**	***S_{BET} (m^2/g)***	***V_{mic} (cm^3/g)***	***V_{meso} (cm^3/g)***	***V_T (cm^3/g)***	***Pore width (nm)***
TWB700	VI	ND	27	0.0124	ND	0.0554	ND
TWAC500	I & IV	H3	160	0.0352	0.205	0.305	7.62
TWAC600	I & IV	H3	301	0.0841	0.213	0.369	4.90
TWAC700	I & IV	H3	334	0.0954	0.362	0.580	6.94
TWAC800	I & IV	H3	103	0.0204	0.185	0.262	10.2
TWAC900	I & IV	H3	58	0.0124	0.193	0.280	19.3

ND – not defined; S_{BET} – BET surface area; V_{mic} – micropore volume; V_{meso} – mesopore volume; V_T – total pore volume

จุฬาลงกรณ์มหาวิทยาลัย
Chulalongkorn University

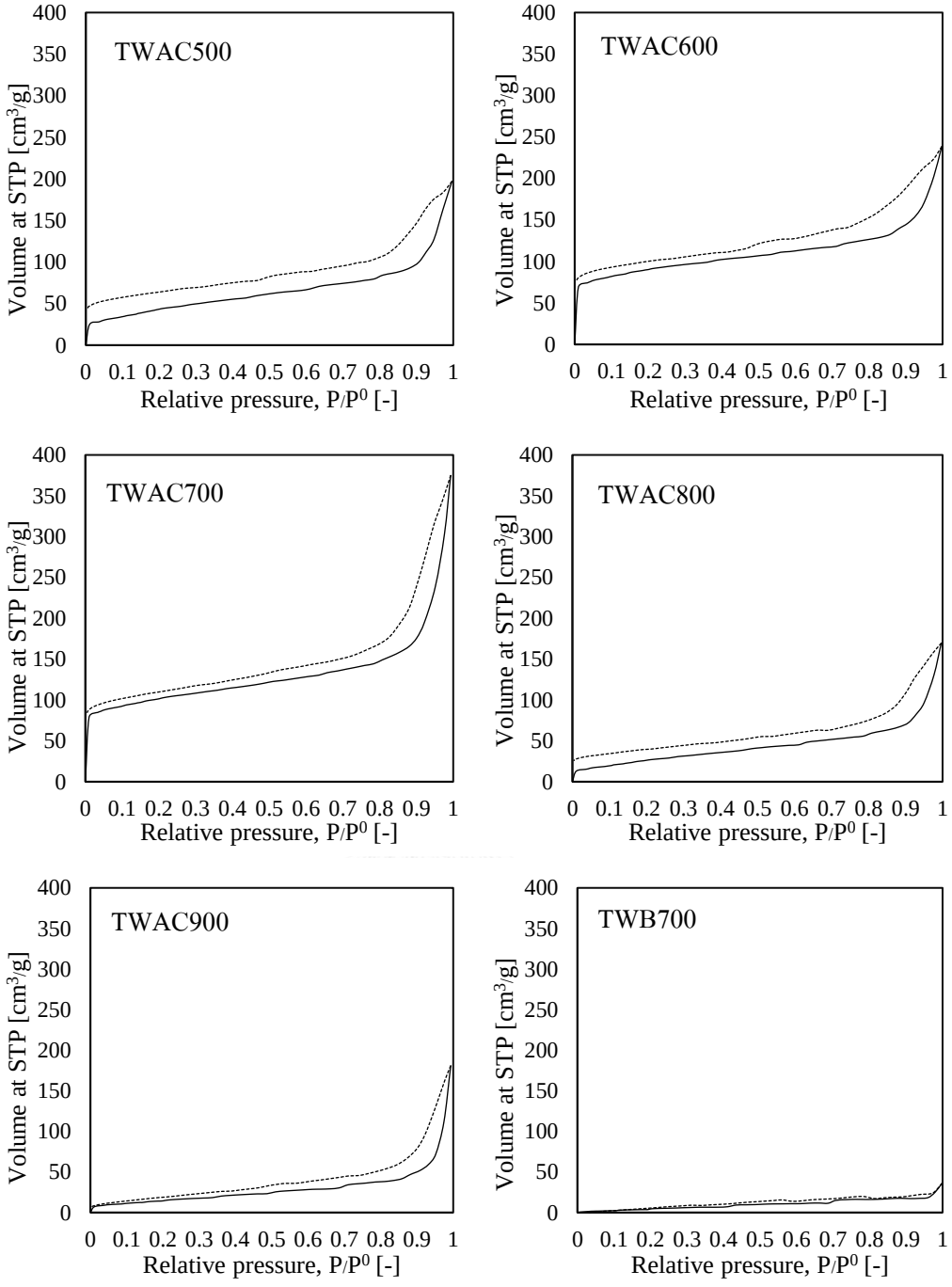

Figure 17 N_2 adsorption and desorption isotherms at 77K of TWAC500-900 and TWB700

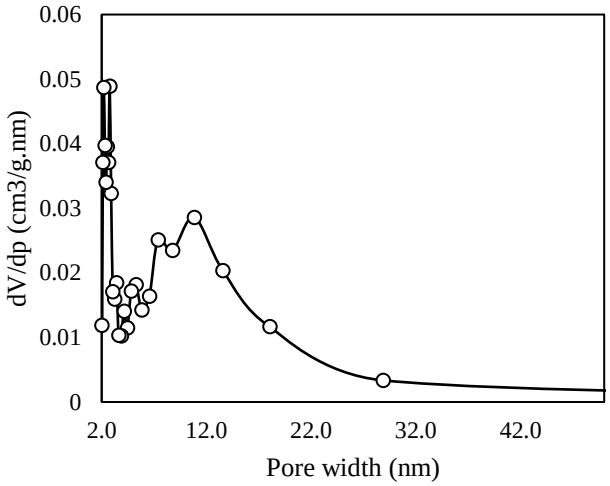

Figure 18 Mesopore size distribution of TWAC700

The pore size distribution of TWAC700 in mesopore width range 2 - 50 nm is displayed in Fig. 18. The pore size distribution, calculated from the desorption data by BJH method, was not uniform. The majority of mesopores were smaller than 4 nm. In addition, for pores larger than 4 nm there was a bell-shaped distribution that peaked at 12 nm and gradually decreased at higher pore width.

Biomass contains different compositions of cellulose, hemicellulose, and lignin which give them different properties. During the carbonization and activation steps, lignocellulosic materials decompose at different rates and temperature ranges. The reactions involved are also rather complex, interconnected and highly dependent on the conditions (activating agent, mass ratio, gas, etc.) [64]. Studies have reported the effect of these lignocellulosic compositions on the porous properties of their char and activated carbon as shown in Table 10. The comparison has some setbacks including the different preparation methods of char and activated carbon, but it could still provide some insights to the roles of cellulose, hemicellulose, and lignin in the production of porous framework. The biomass acts better as a carbon precursor when the lignocellulosic polymers are presented together as evidence by the study of pure cellulose, pure lignin, a mixture of cellulose and lignin as activated carbon in Table 10. The most-developed mesoporous properties were obtained when 50% of cellulose and 50% of lignin was mixed. It was

จุฬาลงกรณ์มหาวิทยาลัย
Chulalongkorn University

suggested that cellulose maintains the mesopore structure while lignin promotes the formation of layered micropore structure during synthesis of activated carbon [65].

In this work, turmeric waste had 58.77% cellulose, 1.24% hemicellulose, and 11.63% lignin by weight. TWAC700 had V_{meso}/V_{mic} equals to 3.79 which could be that the abundant cellulose facilitated the formation of mesopore. It was found that the presence of $CaCl_2$ greatly increased the V_{mic} by 6.70 times and without $CaCl_2$ there was no mesopores. After the coconut shell char was steam activated, the V_{mic} increased by 1.9 times. For plum stone char, steam activation increased the V_{mic} by 5.6 times [66]. From this comparison, $CaCl_2$ activation method increased the V_{mic} and V_{meso} of the char more than steam activation method. At present, it is too complicated to accurately compare and predict the roles of the lignocellulosic compounds in this work to other works because there is no research with the same preparation methods of activated carbon. Also, a certain biomass could favor a type of activation method more than others regardless of the compositions. Further studies on biomass activation by $CaCl_2$ need to be carried out.

จุฬาลงกรณ์มหาวิทยาลัย
Chulalongkorn University

Table 10 Various activated carbon from lignocellulosic materials and their porosity

Sample	Activator	Composition (%w/w)	S_{BET} (m^2/g)	Pore volume (cm^3/g)	Ref.
1. Turmeric waste activated carbon (TWAC700)	$CaCl_2$	Cellulose[a] 58.77% Hemicellulose[a] 1.24% Lignin[b] 11.63%	334	V_T = 0.580 V_{mic} = 0.0954 V_{meso} = 0.362	This work
2. Turmeric waste biochar (TWB700)	-		27	V_T = 0.0554 V_{mic} = 0.0124	This work
3. Date stone activated carbon (FAC)	$FeCl_3$	Cellulose 42% Hemicellulose 18% Lignin 11%	780.06	V_{mic} = 0.468 V_{meso} = 0.105	[67]
4. Date stone activated carbon (ZAC)	$ZnCl_2$		1045.61	V_{mic} = 0.512 V_{meso} = 0.129	[67]
5. Coconut shell char	-	Cellulose 14% Hemicellulose 32% Lignin 46%	NG	V_T = 0.19 V_{mic} = 0.18	[66]
6. Coconut shell activated carbon	Steam		NG	V_T = 0.39 V_{mic} = 0.35	[66]

a - HPLC (Column: VertiSep™ LMP) method, b - NREL/TP-510-42618 method

Chulalongkorn University

Table 10 [continued] Various activated carbon from lignocellulosic materials and their porosity

Sample	Activator	Composition (%w/w)	S_{BET} (m^2/g)	Pore volume (cm^3/g)	Ref.
7. Apple pulp activated carbon	Steam	Cellulose 16% Hemicellulose 16% Lignin 21%	NG	$V_T = 0.44$ $V_{mic} = 0.38$	[66]
8. Plum stone char	-	Cellulose 23% Hemicellulose 20% Lignin 49%	NG	$V_T = 0.05$ $V_{mic} = 0.05$	[66]
9. Plum stone activated carbon	Steam		NG	$V_T = 0.34$ $V_{mic} = 0.28$	[66]
10. Olive “manzanilla” stone activated carbon	Steam	Cellulose 14% Hemicellulose 15% Lignin 42%	NG	$V_T = 0.11$ $V_{mic} = 0.11$	[66]
11. Olive “manzanilla” stone char (H_2SO_4-treated)	-	Cellulose 29% Hemicellulose 20% Lignin 42%	NG	$V_T = 0.16$ $V_{mic} = 0.16$	[66]
12. Olive “manzanilla” stone activated carbon (H_2SO_4-treated)	Steam		NG	$V_T = 0.30$ $V_{mic} = 0.29$	[66]

Table 10 [continued] Various activated carbon from lignocellulosic materials and their porosity

Sample	Activator	Composition (%w/w)	S_{BET} (m^2/g)	Pore volume (cm^3/g)	Ref.
13. Soft wood char	-	Cellulose 36% Hemicellulose 18.5% Lignin 30.5%	NG	$V_T = 0.21$ $V_{mic} = 0.21$	[66]
14. Soft wood activated carbon	Steam		NG	$V_T = 0.54$ $V_{mic} = 0.34$	[66]
15. Pure cellulose activated carbon (AC-1)	$ZnCl_2$ and microwave	Cellulose 100%	1,077.54	$V_T = 0.70$ $V_{mic} = 0.27$ $V_{meso} = 0.43$	[65]
16. Cellulose and lignin activated carbon (AC-2)	$ZnCl_2$ and microwave	Cellulose 78% Lignin 22%	1,041.05	$V_T = 0.87$ $V_{mic} = 0.11$ $V_{meso} = 0.76$	[65]
17. Cellulose and lignin activated carbon (AC-3)	$ZnCl_2$ and microwave	Cellulose 50% Lignin 50%	711.51	$V_T = 1.06$ $V_{mic} = 0.08$ $V_{meso} = 0.98$	[65]

CHULALONGKORN UNIVERSITY

Table 10 [continued] Various activated carbon from lignocellulosic materials and their porosity

Sample	Activator	Composition (%w/w)	S_{BET} (m^2/g)	Pore volume (cm^3/g)	Ref.
18. Cellulose and lignin activated carbon (AC-4)	$ZnCl_2$ and microwave	Cellulose 41% Lignin 59%	615.63	$V_T = 0.93$ $V_{mic} = 0.07$ $V_{meso} = 0.86$	[65]
19. Pure lignin activated carbon (AC-5)	$ZnCl_2$ and microwave	Lignin 100%	558.48	$V_T = 0.54$ $V_{mic} = 0.11$ $V_{meso} = 0.43$	[65]
20. Almond shell activated carbon (ASAC)	$ZnCl_2$ and microwave	Cellulose : Lignin 1 : 1.4	839.60	$V_T = 0.41$ $V_{mic} = 0.15$ $V_{meso} = 0.26$	[65]
21. Macadamia nutshell activated carbon (MNSAC)	$ZnCl_2$ and microwave	Cellulose : Lignin 1 : 1.2	876.80	$V_T = 0.53$ $V_{mic} = 0.42$ $V_{meso} = 0.11$	[65]

จุฬาลงกรณ์มหาวิทยาลัย Chulalongkorn University

4.2.2 Crystalline structure and amorphous structure

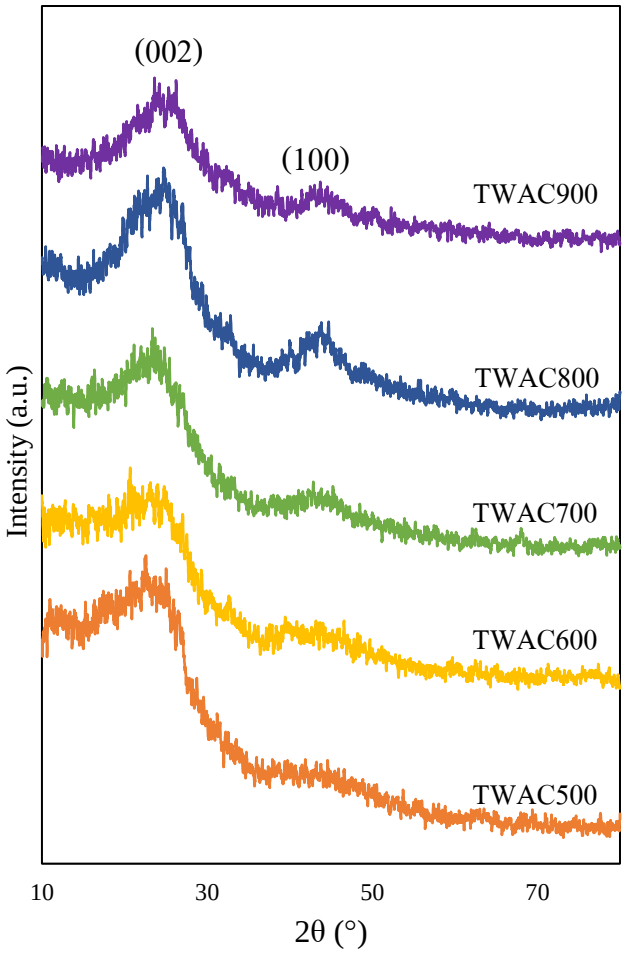

จุฬาลงกรณ์มหาวิทยาลัย
Chulalongkorn University

Figure 19 X-ray diffraction (XRD) patterns of TWAC500-900

The crystal structure of all TWACs was analysed by X-ray diffraction (XRD) as shown in Fig. 19. In all samples, 2 broad peaks appear at 22.6-26.2° and 42.9-43.8° related to the (002) and (100) characteristic peaks of graphite [68, 69]. The broad peaks indicate the samples were amorphous carbon. Furthermore, at higher temperature the peaks are sharper which pertain to the higher degree of graphitization. The patterns also tentatively suggested that the acid washing process effectively removed $CaCl_2$ from the carbons as no peaks of calcium compounds are detected.

4.2.3 Carbon structure by Raman spectroscopy

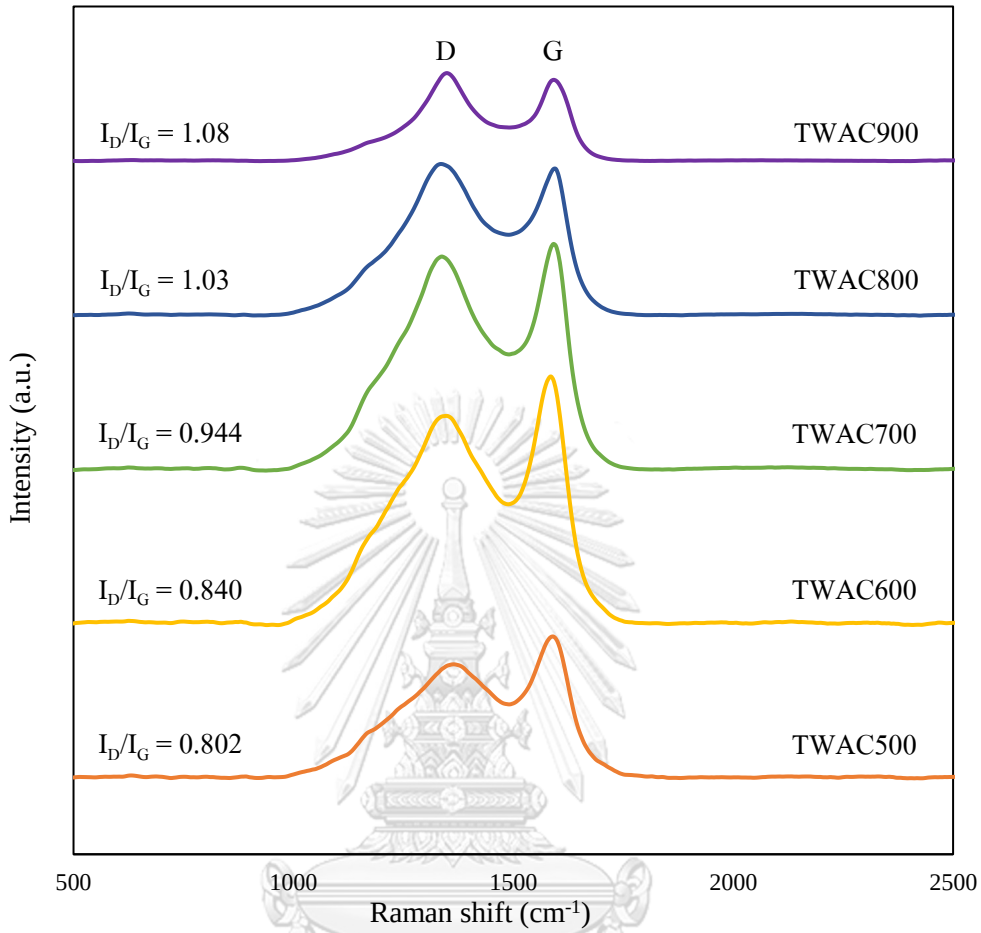

Figure 20 Raman spectra of TWAC500-900

Chulalongkorn University

The structure of partially graphitized carbon was further confirmed by Raman spectroscopy illustrated in Fig. 20. Two broad peaks at 1,337 – 1,367 cm^{-1} and 1,585 – 1591 cm^{-1} are the D-band and G-band, respectively. The peak intensities of the D-band are stronger when the samples were treated at higher temperatures, from 500 to 700 °C, indicating phase transformation from amorphous carbon to a graphitic structure at higher temperature as suggested by the XRD results. This confirms that the higher activation temperature process encouraged the phase formation of graphitic structure.

D-band correlates to the local defects found at the edges of the graphene sheets, while G-band relates to the vibration of sp^2-hybridized carbon in the graphitic hexagonal lattice. The

degree of defects is represented by the intensity ratio of D-band to G-band (I_D/I_G), a higher ratio suggests a higher degree of defects in the graphitic structure [68-70]. The defects could be due to the exposure of more edges during pore formation or the replacement of π bonds (sp^2 carbon atom hybridization) with C-O and/or C-C σ bonds (sp^3). As shown in Fig. 20, TWAC500 has the lowest I_D/I_G at 0.802 and the ratio increased with TWAC900 having the highest I_D/I_G at 1.08. The I_D/I_G ratio increased as the carbonization temperature increased indicating that higher carbonization temperature led to more defects in the graphitic structure.

จุฬาลงกรณ์มหาวิทยาลัย
CHULALONGKORN UNIVERSITY

4.2.4 Morphology and surface texture

Figure 21 SEM images of TWAC500 – 900 at different magnifications

Sample	60x	5,000x	5,000x
TWAC500	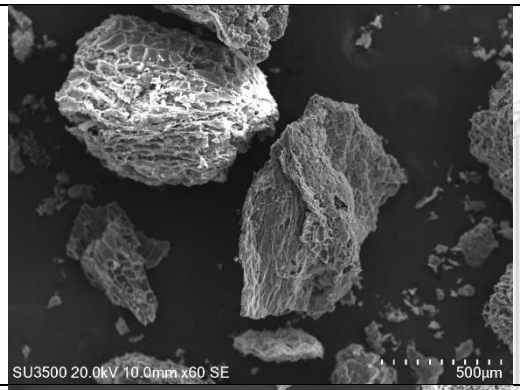	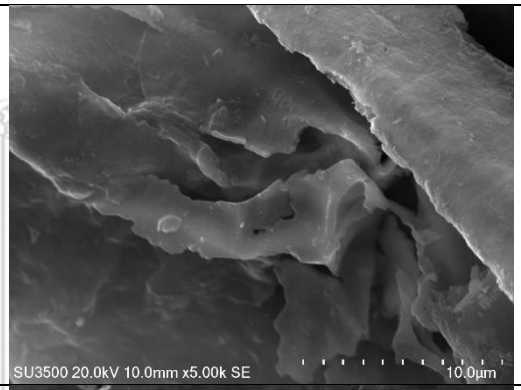	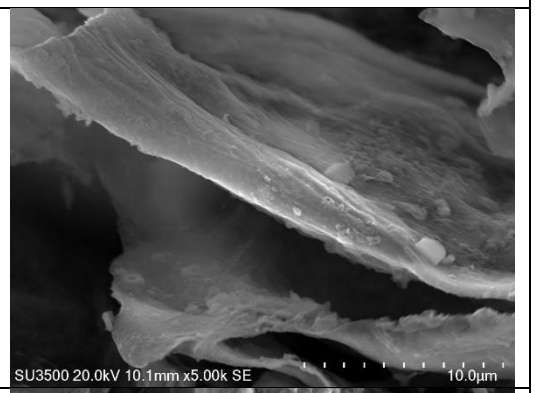
TWAC600	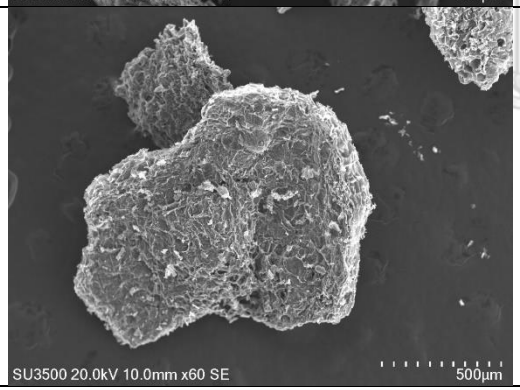	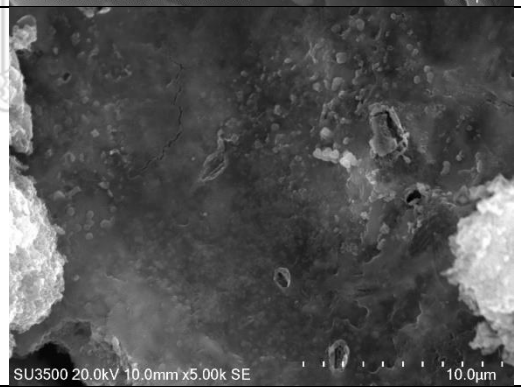	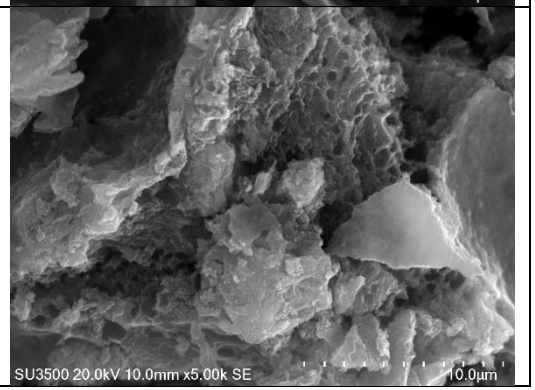

Figure 21 [Continued] SEM images of TWAC500 – 900 at different magnifications

Sample	60x	5,000x	5,000x
TWAC700	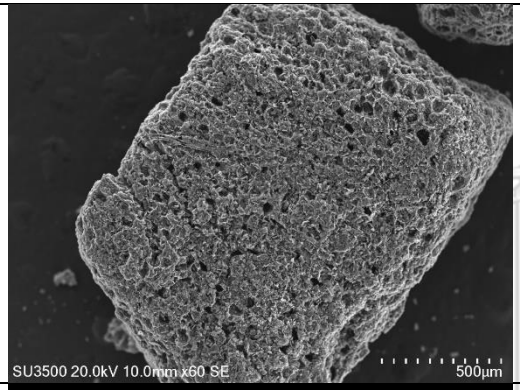	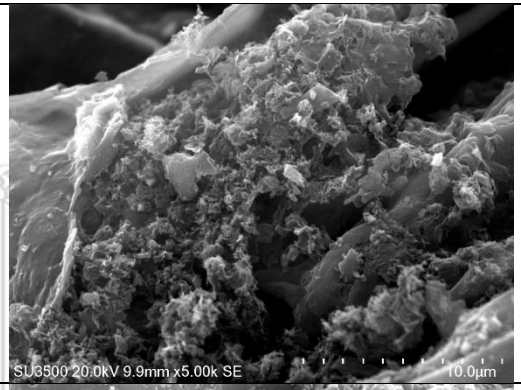	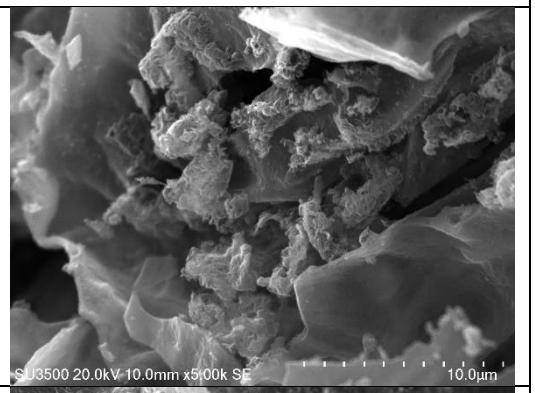
TWAC800	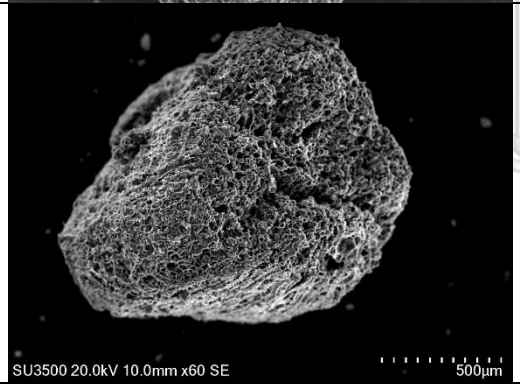	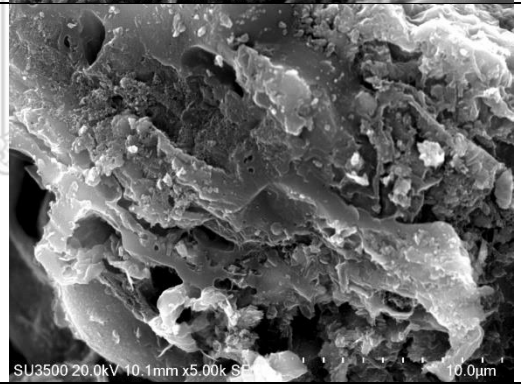	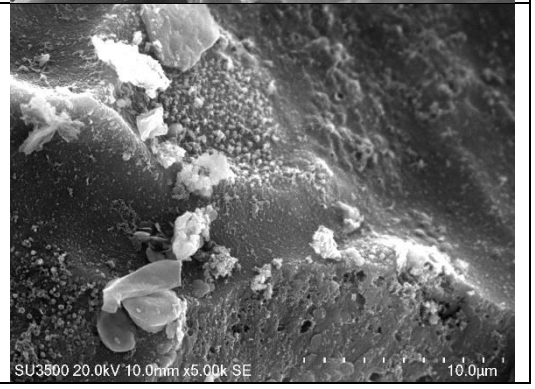

Figure 21 [Continued] SEM images of TWAC500 – 900 at different magnifications

Sample	**60x**	**5,000x**	**5,000x**
TWAC900	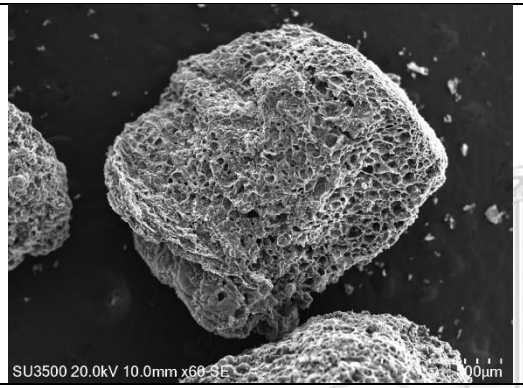	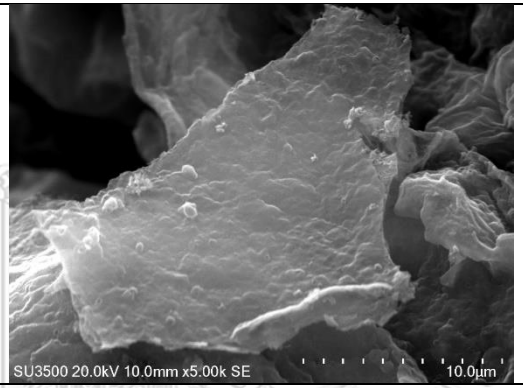	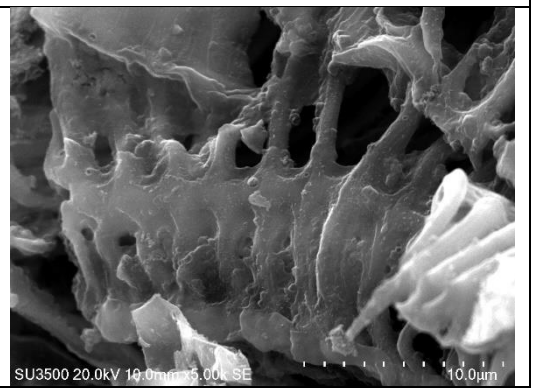

The morphology and surface properties of TWAC500 – 900 are illustrated in Fig. 21. At 60x magnifying power, the image of a single particle of activated carbon was captured. The surface of the carbons is rough and porous. At 5,000x magnifying power, the images were taken in 2 areas for every TWAC, and the images show that the pores are highly non-uniform. TWAC500-900 presented similar texture across all activation temperature. In some areas, it is smooth, while other areas of the same carbon are coarse and filled with deep crevices.

The SEM-EDX results of 3 different areas of TWAC700, as summarised in Table 11, revealed the presence of C, O, Ca, Cl. The results explained further that despite the absence of crystalline form of calcium and chloride phases in the XRD patterns in section 4.2.2 crystalline structure, leftover Ca and Cl were still presence in the carbon. In addition, TWAC700 comprised of less than 90 %Weight of C. The presence of these elements was well distributed in the 3 areas.

Table 11 Chemical compositions of TWAC700 characterized by SEM-EDX

Element	**Area 1**		**Area 2**		**Area 3**	
	%Weight	**%Atom**	**%Weight**	**%Atom**	**%Weight**	**%Atom**
C	88.24	92.97	87.48	92.34	86.53	91.38
O	6.77	5.35	7.55	5.98	8.96	7.11
Cl	2.44	0.87	2.58	0.92	2.17	0.78
Ca	2.56	0.81	2.39	0.76	2.34	0.74
Total	100.00	100.00	100.00	100.00	100.00	100.00

จุฬาลงกรณ์มหาวิทยาลัย
CHULALONGKORN UNIVERSITY

4.2.5 Surface functional groups

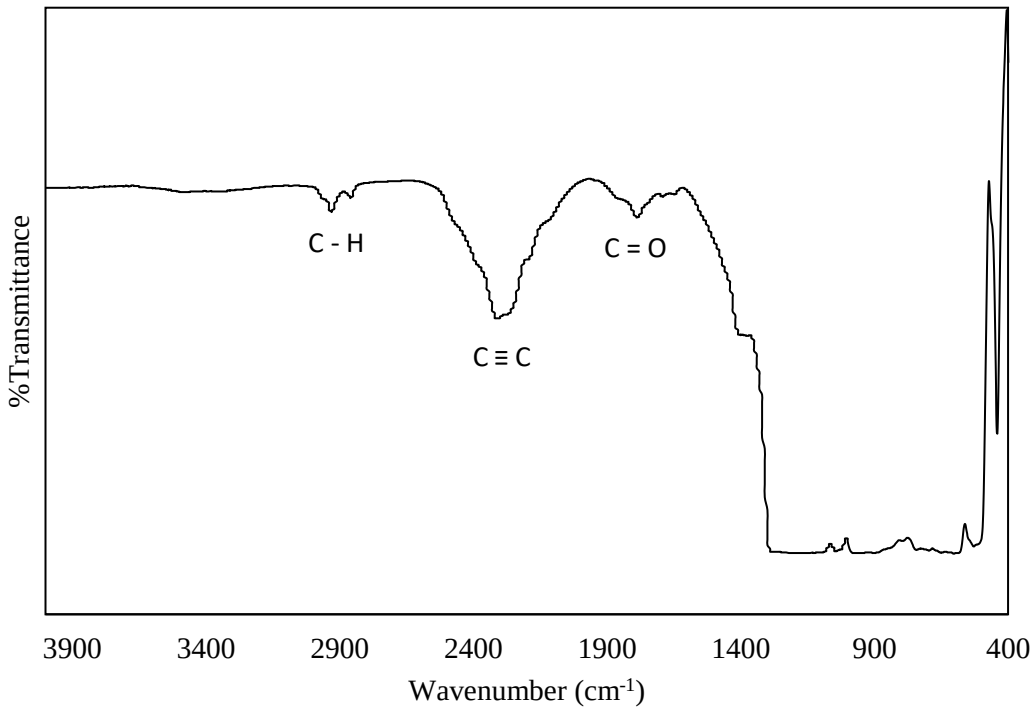

Figure 22 FTIR spectra of TWAC700

Before TWAC700 would be used to study NOR adsorption, Fourier transform infrared spectroscopy technique was applied to analyse the surface functionality of the adsorbent. Fig. 22 illustrates the FTIR spectra of TWAC700 between wavenumber 4000 – 400 cm^{-1}. Fingerprint region is the region below 1,500 cm^{-1} where a lot of the absorbance from bending vibrations are seen. Therefore, in this work, the FTIR was interpreted in the wavenumber 4000 – 1,500 cm^{-1}. The highest intensity peak is at 2320 cm^{-1} attributed to the C $\equiv$ C stretching vibrations in alkyne groups. The band at 1793 cm^{-1} refers to the stretching vibrations of C = O denoting the existence of carbonyl/carboxyl groups. Lasty, the weak bands at 2800 – 3000 cm^{-1} suggests the presence of an aliphatic C-H stretching [71].

4.3 Norfloxacin adsorption

From the previous section, TWAC700 was chosen as the adsorbent because it had the highest V_{meso} ,S_{BET} and V_{mic} out of all the TWACs. (A comparative NOR adsorption test between TWB700 and TWAC500 – 900 had been conducted and verified TWAC700 as the best adsorbent, results can be found in the Appendix in Fig. 35-36) All NOR adsorption studies in this work were done using only TWAC700.

4.3.1 Effect of carbon dosage

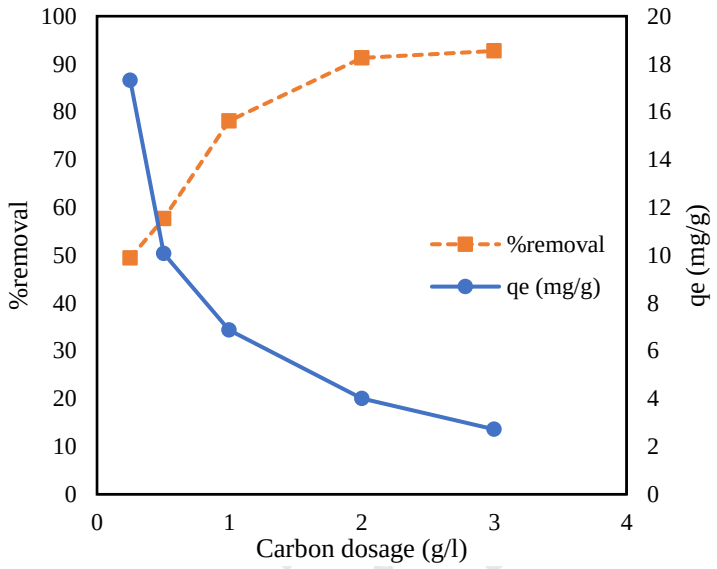

จุฬาลงกรณ์มหาวิทยาลัย
CHULALONGKORN UNIVERSITY

Figure 23 Effect of carbon dosage on the %removal and q_e of NOR

The effect of adsorbent dose for NOR adsorption was investigated using various amounts of TWAC700 from 0.25 to 3 g/l in 100 mL of 10 mg/l NOR at 25°C, 24 h. The adsorption data are reported in Fig. 23 in two terms; removal percentage (%removal) in orange squares, left y-scale, and NOR uptake (q_e) in blue circles, right y-scale. The %removal was 43.7 - 96.1 percent with 3 g/l dose giving the highest %removal at 96.1 percent. This was because as TWAC700 dosage increased the number of active sites also increased allowing more NOR to be removed. On the contrary, q_e obtained from the same experiment was 2.82 - 15.0 mg/g with 0.25 g/l dose resulting in the highest q_e. The trend of q_e versus carbon dosage was descending due to the limited adsorbate molecules available in water as carbon dosage increased [72]. The following

adsorption experiments would be conducted with 1 g/l TWAC700 dosage because of reasonable removal percentage (78.4%) and q_e value (6.90 mg/g).

4.3.2 Effect of initial concentration

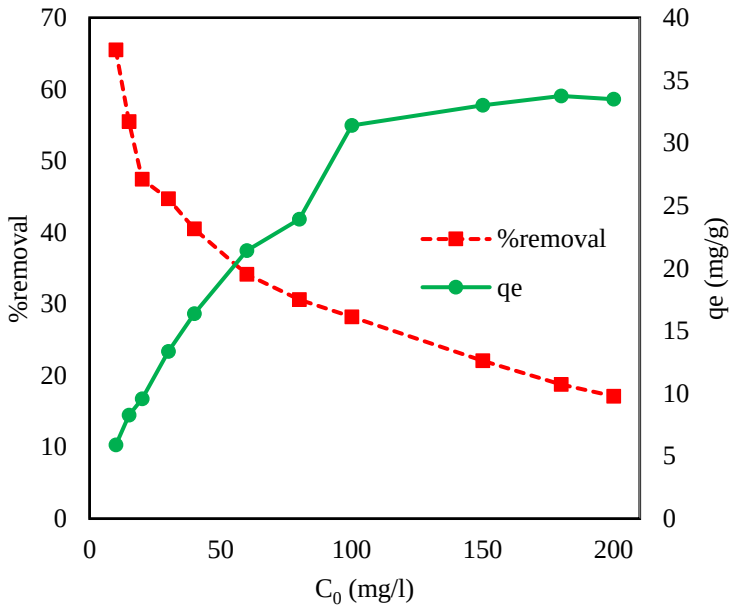

Figure 24 Effect of C_0 (initial concentration) on the %removal and q_e of NOR

The effect of initial concentration on NOR adsorption was studied under varying initial concentrations of NOR from 10 to 200 mg/l at 25 °C, 24 h. The TWAC700 dosage was fixed at 1 g/l. The adsorption data are reported in Fig. 20 in two terms; removal percentage (%removal) in red squares, left y-scale, and NOR uptake (q_e) in green circles, right y-scale. The %removal was 17.1 – 65.5 percent in descending trend as initial concentration increased. On the contrary, the q_e increased as the initial concentration increased until after C_i = 100 mg/l, the change in q_e was insignificant. At lower initial NOR concentrations, the available adsorption sites were relatively high compared to higher concentrations, thus the majority of NOR was removed resulting in high removal percentage. At higher initial concentrations, the pores filled up with NOR molecules leading to a decrease in removal percentage of NOR. However, the higher initial concentrations had higher driving force attributing to an increase in q_e [73].

4.3.3 Adsorption equilibrium

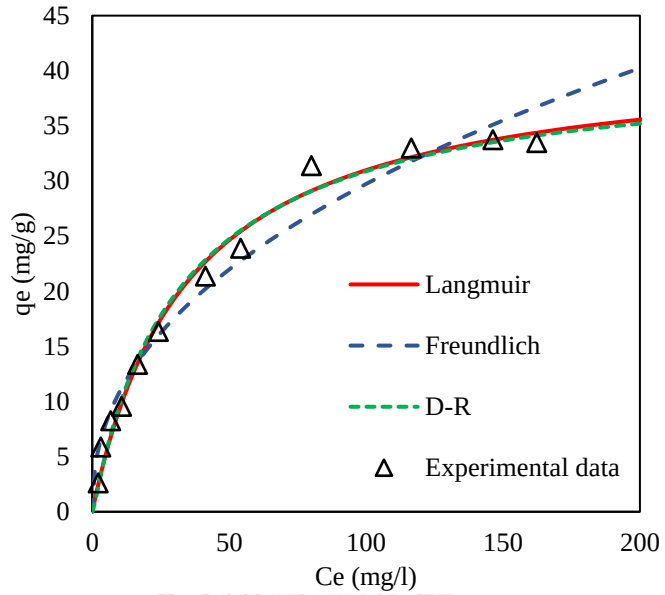

Figure 25 Isotherm fitting curves for NOR adsorption onto TWAC700 and experimental data

The NOR adsorption data by TWAC700, 5 – 200 mg/l of NOR at 25 °C, and carbon dosage 1 g/l was further investigated by adsorption isotherm models. Langmuir, Freundlich, and D-R isotherms were employed to analyse the adsorption mechanism by fitting the experimental data using nonlinear regression method. The resulting isotherm parameters and correlation coefficients were shown in Table 12, and the fitted curves along with the experimental data was illustrated in Fig. 25. The equilibrium data was found to be in accordance with Langmuir isotherm the most as it gave the highest R^2 of 0.9866. Followed closely by the D-R model at R^2 = 0.9853, the 2 curves (red solid line for Langmuir, green dotted line for D-R) are nearly identical. Freundlich isotherm was the least fitted at R^2 = 0.9674. The equilibrium isotherms suggested that the adsorption mechanism was monolayer onto homogeneous sites rather than multilayer onto heterogeneous sites. The maximum monolayer adsorption capacity (q_m) calculated by Langmuir model was 41.7 mg/g which is higher than some of the biomass-based activated carbon in literature (Table 6). All R^2 values and parameters calculated by Langmuir (q_m, K_L), Freundlich (K_F, n), and D-R (q_{DR}, E) models are displayed in Table 11.

จุฬาลงกรณ์มหาวิทยาลัย
Chulalongkorn University

D-R model could give information about the type of adsorption through term E (kJ/mol), adsorption energy. E value can distinguish the adsorption mechanism. E < 8 is physical adsorption, 8 < E < 16 is chemical adsorption, E > 16 is ion exchange. It should be noted that D-R model was the only regression that was done under unit mol of NOR, as opposed to Langmuir and Freundlich where mg of NOR was used. In this work, E value was 5.18 kJ/mol which is less than 8 kJ/mol, therefore; the adsorption mechanism of NOR was purely physisorption.

Table 12 Langmuir, Freundlich, and D-R isotherm parameters for NOR adsorption

Model	Parameter	Value
Langmuir	q_m (mg/g)	41.7
	K_L (l/mg)	0.0288
	R^2 (-)	0.9866
Freundlich	K_f (mg/g)(l/mg)$^{1/n}$	3.98
	n (-)	2.29
	R^2 (-)	0.9674
D-R	q_{DR} (mg/g)	39.1
	E (kJ/mol)	5.18
	R^2 (-)	0.9853

จุฬาลงกรณ์มหาวิทยาลัย
CHULALONGKORN UNIVERSITY

Additionally, R_L was calculated from Langmuir parameter K_L by eq (4) with C_0 at 0 – 200 mg/l as shown in Fig. 26. R_L was lower than 1 and descends as the initial concentration increases indicating that as initial concentration increases the adsorption gets more favourable.

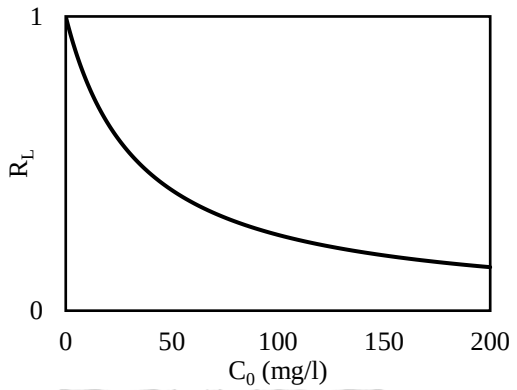

Figure 26 R_L value across C_0 (initial concentration) = 0 – 200 mg/l

จุฬาลงกรณ์มหาวิทยาลัย
CHULALONGKORN UNIVERSITY

4.3.4 Adsorption kinetics

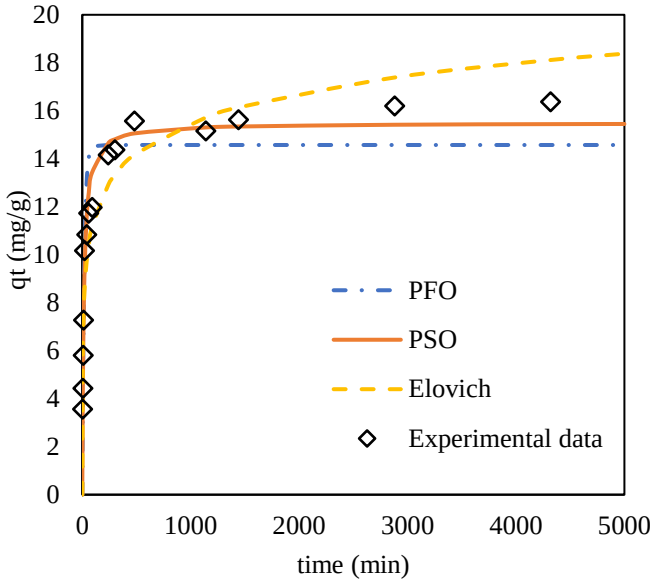

Figure 27 Kinetic models fitting curves for NOR adsorption onto TWAC700 and experimental data

Fig. 27 shows kinetic of adsorption nonlinear fitted curves at a temperature of 25 °C, TWAC700 dosage of 1 g/l, and initial concentration of NOR 40 mg/l. The adsorption reached near equilibrium after 4 h. PFO, PSO, and Elovich kinetics models were applied to study the mechanism behind the adsorption rate. R^2 values and kinetics parameters from PFO (k_1, q_{e1}), PSO (k_2, q_{e2},h), and Elovich (α, β) model regression are listed in Table 13. PSO fitted the data the most from its significantly higher R^2 at 0.9733. PFO and Elovich models both had R^2 values around 0.9. This suggested that the pseudo-second-order kinetic model best described the adsorption process of NOR.

จุฬาลงกรณ์มหาวิทยาลัย
Chulalongkorn University

Table 13 Pseudo-first-order (PFO), pseudo-second-order (PSO), and Elovich kinetic parameters for NOR adsorption

Model	Parameter	Value
PFO	k_1 (1/min)	0.0551
	q_{e1} (mg/g)	14.6
	R^2 (-)	0.9013
PSO	k_2 (g/mg·min)	0.00465
	q_{e2} (mg/g)	15.5
	h (mg/g·min)	1.12
	R^2 (-)	0.9733
Elovich	α (mg/g·min)	9.75
	β (g/mg)	0.555
	R^2 (-)	0.9078

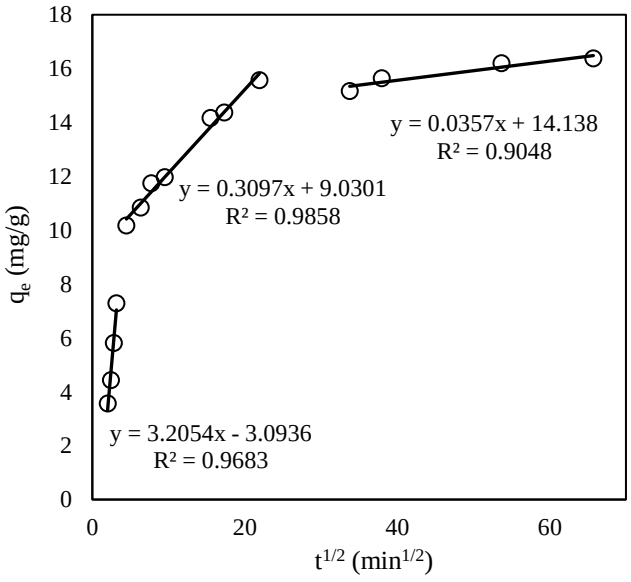

Figure 28 Intraparticle diffusion model regression for NOR adsorption onto TWAC700

The intraparticle diffusion model using linear regression is shown in Fig. 28. The intraparticle diffusion model is used for determining the adsorption mechanism and rate-limiting step. If the regression of q_t versus $t^{1/2}$ is a straight line and passes through the origin, intraparticle diffusion is the rate-limiting step, according to Weber and Morris [45]. From Fig. 28, the regression is divided into 3 sections, none of which passes throught the orgin. Consequently, the adsorption occurred in 3 steps: (i) boundary-layer diffusion of NOR; (ii) intraparticle diffusion which is slower than the first step; and (iii) equilibrium stage where adsorption gradually approahed completion [74]. R^2 value and other parameters (k_i, C_i) are listed in Table 14. In conclusion, the intraparticle diffusion was not the sole rate-limiting step. The rate-limiting steps were a combination of film diffusion and intraparticle diffusion instead.

Table 14 Intraparticle diffusion parameters

Steps	**k_i (mg/g·min$^{1/2}$)**	**C_i (mg/g)**	**R^2**
Step 1	3.21	-3.09	0.9683
Step 2	0.310	9.03	0.9858
Step 3	0.0357	14.1	0.9048

จุฬาลงกรณ์มหาวิทยาลัย
CHULALONGKORN UNIVERSITY

4.3.5 Thermodynamics of adsorption

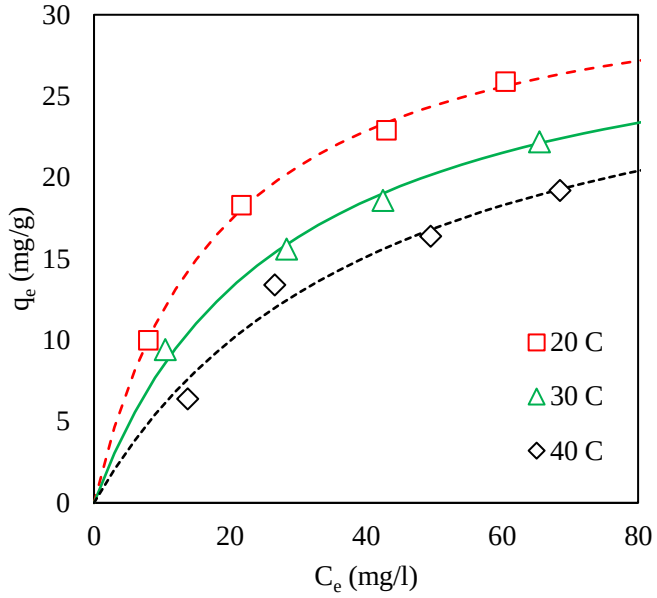

Figure 29 Langmuir isotherm fitting curves for NOR adsorption at 20 – 40 °C, C_0 = 20 – 80 mg/l

To further investigate the thermodynamics of adsorption from D-R isotherm in Section 4.3.3 Adsorption equilibrium, another experiment was carried out at 3 temperatures of 20 - 40 °C, TWAC700 dosage of 1 g/l, and initial concentration of NOR 20 - 80 mg/l. As displayed in Fig. 25, the experimental data was fitted with Langmuir isotherm, Langmuir nonlinear regression parameters are given in Table 14. K_L from Langmuir isotherm was then used to calculate the K_c via eq (19) to be plotted against 1/T as shown in Fig. 26. ΔH and ΔS were obtained from the slope and y-intercept of the linear regression, the values (ΔH, ΔS, ΔG) are summarized in Table 15.

The negative value of ΔH (-32.0 kJ/mol) revealed that the adsorption process was exothermic and more favourable at low temperatures which can be confirmed by Fig 25. Moreover, the magnitude of ΔH can reveal the mode of adsorption. If the magnitude of $\Delta H < 84$ kJ/mol, the mechanism is physical adsorption. If $80 < \Delta H < 420$ kJ/mol, it's chemical adsorption [70]. In this case, $\Delta H < 84$ kJ/mol meant the adsorption is physical adsorption. The positive value of ΔS (5.50 J/mol·K) disclosed that there was an increase in the degree of freedom of NOR after

the adsorption process. The negative values of ΔG at each temperature showed that the adsorption was spontaneous and feasible. The ΔG values were nearly equal at each temperature because the ΔS value used to calculated ΔG was very small.

Table 15 Langmuir adsorption isotherm parameters at 20, 30, 40 °C

Temperature (°C)	q_m (mg/g)	K_L (l/mg)	R^2
20	33.5	0.0537	0.9997
30	31.5	0.0359	0.9992
40	31.4	0.0232	0.9600

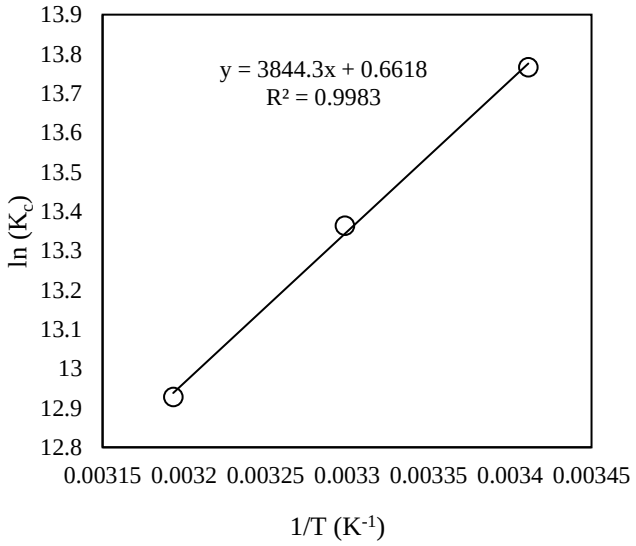

Figure 30 Plot of ln(K_c) versus 1/T (K^{-1})

Table 16 NOR adsorption thermodynamics parameters

T (K)	ΔG (kJ/mol)	ΔH (kJ/mol)	ΔS (J/mol·K)
293.15	-33.6	-32.0	5.50
303.15	-33.6		
313.15	-33.7		

4.3.6 TWAC as NOR adsorbent compared to other biomass-based materials

This work is the first ever to use turmeric waste activated carbon to adsorb Norfloxacin or any pharmaceuticals. In addition to that, it is uncommon but desirable to report the porosity data in terms of different pore sizes (micropore, mesopore) since they are integral to the adsorption capacities. Commercially, activated carbons on the market are measured and sold by only their BET surface area which is inadequate to fully comprehend the porous properties. An example of the properties of commercial activated carbon synthesized from coconut shell is shown in Fig. 26. The volume of micropores and mesopores were not mentioned. Commercial activated carbon might report high surface area, but it is mostly due to an abundance of micropores. The desirable mesopores for organic compound adsorption result in lower BET surface area. Therefore, it is not enough to judge the effectiveness of activated carbon by BET surface area, micropore and mesopore volumes are required. Additionally, according to a finding, typical commercial activated carbons have mesopore volume around 0.1 – 0.5 cm^3/g [75], TWAC700 has mesopore volume at 0.362 cm^3/g. Lower BET surface area at 334 m^2/g was due to the majority of pores being mesopores rather than micropores.

จุฬาลงกรณ์มหาวิทยาลัย
Chulalongkorn University

CARBOKARN GRADES

The Carbokarn range of typical Coconut Carbons can be supplemented with a decolorising "Hi-molecular Wt organics adsorbing" category of carbon made from an alternative raw material available in abundance.
This Bulletin provides elementary data on properties of Carbokarn standard product range, to which speciality carbons are progressively added. More comprehensive literature on Activated Carbon, specific application related performances, properties & specifications of individual grades, Test methods and samples, are available on request to bona-fide users. Although standardised mainly on A.S.T.M/A.W.W.A. test methods Carbokarn is equipped to conduct evaluations on CEFIC/DIN, JIS, US Military Procedures,as well as most application oriented tests.

Range of Properties	Test Method D = ASTM	Description (Also refer graphically presented information in folder)	Units	Value Range depending on grade
Particle sizes (US Sieves) -Standard	D 2862-82	4/8, 6/12, 6/16, 8/16, 8/30, 12/20, 12/40, 20/50, 30/200, M200, M325	% WW retained	Too numerous
(E 22-82) - Specials	D 2862-82	4/6, 4/10, 6/10, 8/14, 8/20, 12/30, 14/40, 16/25, 30/60, 30/140, Others	on sieve	to specify
Mean Particle Diameter	AWWA B604-74	Depends on particle size and distribution	mm	0.02 to 4.15
Uniformity Coefficient	AWWA B604-74	" " "	-	1.1 to 2.1
Voids in dense packed bed	CARBOKARN	Influenced by particle shape/size	% v/v	39 to 42
Density - Apparent (dry)	D2854-83	Vibrated uniform fall; value varies inversely with activity	g/cc	0.34 to 0.60
Density - Particle	Hg.displacement	Wt. of carbon per unit volume excluding volume of voids	g/cc	0.57 to 1.00
Density - Real	He.displacement	Density of carbon matter exculding voids & pore volume	g/cc	2.2
Density - Wetted	CARBOKARN	Weight of carbon and adhering water/unit volume; wetting 24 hrs.	g/cc	1.20 to 1.30
Density - Backwashed & drained	CARBOKARN	Dry weight of carbon/volume when backwashed & drained	g/cc	0.32 to 0.57
Moisture	D2867-83	As packed and priced: Granules max 8%; Powders max 12%	% W/W	Gran 4-6
pH	D3838-80	Of standard grades. (Adjusted types available)	-	8.5 - 10.5
Specific Heat		@ 100 °C; per °C	Cal/g	0.25
Ignition Temperature	D3466-76	Untreated Carbons: (specials 450°C +)	°C	350+
Ash	D2866-83	Standard Grades: (Specials 0.2-0.6)	% W/W	1.5 to 5.0
% water soluble	CARBOKARN	"	% W/W	0.5 to 2.5
% acid soluble	CARBOKARN	"	% W/W	1.0 TO 3.5
Chlorides	CARBOKARN	"	ppm	500 max
Sulphur	BS 1016 : PART 6	"	ppm	1000 max
Iron	CARBOKARN	"	ppm	1500 max
Hardness Number	D3802-79	% retained after 1/2-hr agitation with steel balls	%	98-99.5
Abrasion Number - Rotap	AWWA-B604-74	% retention original MPD after 1/3-hr agitation with steel balls	%	87-97
" " - Stiming	" "	% retention original MPD after 1-hr Mechanical Pressure & Stiming	%	90-99
Wet Attrition Test (Denver Cell)	MINTEK	Udersize on 1-hr agitation at 1200 rpm, in water	% W/W	5-8 to 10-12
Carbon Tetrachloride Adsorption	D3467-88	Max wt. adsorbed from satd stream at 1670 ml/min at 25 °C	% W/W	20 to 110
" " Retention	CARBOKARN	Residual not desorbed at 2000 ml/min.air 1 hr at 25 °C	% W/W	15 to 80
Benzene adsorption 100% Satn	JIS 1474-75	Max Wt adsorbed from satd stream at 1350 ml/min @ 25 °C	% W/W	24 to 60
" " 10% "	"	Max Wt adsorbed from 1/10 satd gas/air stream @ 1500 ml/min @ 25 °C	% W/W	22 to 51
Acetone	"	Max Wt adsorbed from satd stream at 1350 ml/min @ 25 °C	% W/W	21 to 51
Methylene Blue	JIS K 1470-67	Volume of standard MB solution adsorbed per g AC	cc/g	100 to 300
Iodine Number	D 4607-86	Wt. of Iodine adsorbed per g AC at 0.02N residual Iodine conc.	mg/g	800 to 1600
Surface Area	C 819-77	Based on B.E.T. Nitrogen Method	m^2/g	800 to 1600
Phenol	DIN 19603	Capacity at 1 mg/litre residual conc.	% W/W	4 to 8
Phenol	AWWA B600-78	Conc. of AC needed to reduce Phenol conc. from 200 to 20 mg/litre (Powder)	g/l	1.0 to 3.0
Phenol	AWWA B604-74	Adsorption Capacity from 5g/litre solution (Granules)	% W/W	50-90
Gold Kinetics	MINTEK ANALYSER	Residual conc. after 90 mins, of a 100 ppm gold solution	ppm	5-20
Gold Equilibrium Capacity	CIP Tests	Gold loading on AC in equilibrium with 1 gm Au/ton solution	mg/g	25-35
Dechlorination Half Value	DIN 19603	Height of AC layer to halve inlet conc. 5 ppm at 1 cm/sec flow	cms	1 to 5
" Capacity	CARBOKARN	10 ppm inlet; Gallons @ 1 GPM/ft^2 for 0.01 ppm break through	Gal/ft^3 AC	$2x10^5$ (min)

POPULAR GRADES Standard Unimpregnated Types : In same field of application 10 - 20 alternative grades may be used, depending on individual customer need.
Special impregnated types can also be supplied on request.

Precious Metals Recovery - 6/12, 6/16, 8/16, (CIP/CIL), 12/30 & 12/40 (Columns), M325 (Flotation) - TN5, HR5, PHO, PH5, YAO
Gas/Air Purification - 6 mm/8 mesh, 4/6, 4/8, 4/10, 6/12 - DEO, HRO, PHO, YAO
Solvent Recovery - 4/8, 6/12 - YAO, HT5 (including acid washed grades)
Safety Masks & Respirators - 8/14, 12/20 - PHO, YAO, HTO, HT5, ATO, NVO
Military Suits - M325 YAO, ATO
Adsorbent Foams - M325 - TNO, PH5
Nuclear Industry - 6/14, 8/16 - YAO, PH5 (impreg. for Radio Iodine), DEO, TNO (Noble Gas Delay)
Electroplating Solutions - 12/20, 12/30, 20/50, M200 - PH5, YAO
Dechlorination/Taste/Odour in water - 8/30, 12/30, 12/40, 14/45, 20/50 - HRO, PHO, YAO
Aquariums - 4/8 DE5
Catalyst & Catalyst suport - 6/12, 8/16, 12/20 - HTO, ATO
Cigarette Filters - 14/40, 16/25, 20/50 - YAO, HT5
Trace Organics in water - 12/30, 14/40, 20/50, M200 - HRO, PHO, YAO

Figure 31 Carbokarn's commercial activated carbon grades [76]

Table 16 summarizes a comparison of the porous properties and the maximum monolayer adsorption capacity (q_m). The q_m value for TWAC700 was 41.7 mg/g which was higher than some of the adsorbents in literature. Moreover, NOR adsorption by TWAC700 was conducted at neutral pH which is considered environmentally friendly since no added chemical is required for pH adjustment. Notedly, biochar derived from *Luffa* sponge reported q_m as high as 278.0 mg/g at 25 °C which could be attributed to its high surface area (822 m^2/g) and – OH functional group on the surface. The high surface area of *Luffa* sponge biochar could be from its composition: 82.4% cellulose and 11.2% lignin, and activation method: H_3PO_4 [57]. Granular activated carbon from maize straw which reported q_m at 112.8 mg/g, the good adsorption capacity could be attributed to the high micropore, and total pore volume of the sample (V_T = 1.31 cm^3/g, V_{mic} = 0.13 cm^3/g) [56].

Turmeric waste activated carbon was synthesized from an agrilcultural waste in support of the BCG business model. Interestingly, compared to other biomass, turmeric waste is exceptionally clean because it was collected from a pharmaceutical production line. Turmeric waste was abundant and easy to collect from one location. This work is the first step to adding value to turmeric waste and finding its application. The high V_{meso} of TWAC700 (0.362 cm^3/g) is an attractive asset to further explore the adsorption of other emerging pollutants.

จุฬาลงกรณ์มหาวิทยาลัย
CHULALONGKORN UNIVERSITY

Table 17 List of group 3 biomass-based adsorbents and group 4 commercial activated carbons from Table 6 and their NOR adsorption capacities compared to this work

Adsorbent	S_{BET} (m^2/g)	Pore volume (cm^3/g)	Pore size (nm)	q_m (mg/g)	Ref
Group 3 Biomass-based materials					
1. Turmeric waste activated carbon (TWAC700)	334	$V_T = 0.580$ $V_{mic} = 0.0954$ $V_{meso} = 0.362$	6.94	41.7	this work
2. Pomelo peel-based biochar	1.71	$V_T = 0.003$	5.90	34.88	[53]
3. Cauliflower roots biochar	232	$V_T = 0.15$ $V_{mic} = 0.07$ $V_{meso} = 0.08$	-	31.15	[19]
4. Cassava waste KOH-modified biochar	128	$V_T = 0.010$	2.42	1.960	[54]
5. Corn activated magnetic biochar	761	$V_T = 0.37$	-	7.247	[49]
6. Reed activated magnetic biochar	778	$V_T = 0.33$	-	3.514	[49]
7. Willow activated magnetic biochar	857	$V_T = 0.40$	-	6.259	[49]
8. Hematite-reed straw biochar composites	135	$V_T = 0.086$	2.54	4.074	[55]
9. Pyrite-reed straw biochar composites	54.5	$V_T = 0.053$	3.90	5.106	[55]
10. Granular activated carbon from maize straw	1200	$V_T = 1.31$ $V_{mic} = 0.13$	-	112.8	[56]
11. Biochar derived from *luffa* sponge	822	-	5.35	278.0	[57]
Group 4 Commerical activated carbons					
12. Commercial activated carbon from wood charcoal (Fisher Scientific)	664	-	-	112.5	[48]
13. Commercial powder activated carbon (mesh 200 ground Filtrasorb-400, Calgon Corp., USA, $1.49 per pound)	-	-	-	237	[58]

จุฬาลงกรณ์มหาวิทยาลัย
Chulalongkorn University

Chapter 5

Conclusions

This thesis focused on the preparation of turmeric waste activated carbon as the adsorbent to NOR. This chapter concludes all the experiments and findings divided into 2 parts below.

5.1 Activated carbon synthesis

Turmeric waste activated carbon was synthesized by simultaneous carbonization and chemical activation using $CaCl_2$. The carbonization was studied across temperature 500 - 900 ˚C to find the optimal carbonization temperature for highest mesopore volume. The turmeric waste activated carbon carbonized at 700 ˚C (TWAC700) had the highest mesopore volume at 0.362 cm^3/g, specific surface area 334 m^2/g, and micropore volume 0.0954 cm^3/g. $CaCl_2$ played an important role in the chemical activation process as it was shown to produce mesopore and enhance surface properties. Without $CaCl_2$, turmeric waste biochar (TWB700) yielded significantly lower porosity without mesopores at surface area 27 m^2/g, total pore volume 0.0554 cm^3/g, and micropore volume 0.0124 cm^3/g.

จุฬาลงกรณ์มหาวิทยาลัย
Chulalongkorn University

The texture of TWAC500-900 was not significantly different. The TWAC700 consisted of almost 90% carbon and the rest were oxygen that was not completely gasified, calcium and chlorine residues from acid washing process during preparation. The structure of TWAC500 – 900 was partly graphitized.

Since TWAC700 presented the best mesopore volume, micropore volume, and surface area, it was chosen as the Norfloxacin adsorption in the next part.

5.2 Norfloxacin adsorption by activated carbon

TWAC700 was used to study the Norfloxacin adsorption. It was found that 4 g/l of TWAC700 could remove 92.7% of 10 mg/l Norfloxacin. In the adsorption isotherm study, it was best fitted with Langmuir adsorption model by nonlinear regression which implied that the adsorption was monolayered and occurred on a homogeneous surface. At pH 7, 25 ˚C, the maximum monolayer adsorption capacity was 41.7 mg/g. D-R model revealed that the adsorption is a physical adsorption. In the adsorption kinetics study, it was found that the rate of adsorption was described by pseudo second order kinetics, and the rate-limiting steps were a combination of boundary layer diffusion and intraparticle diffusion. The adsorption approached near equilibrium after 4 h. From the thermodynamics study, the adsorption was further confirmed as physical adsorption. The process was exothermic, at lower temperature the adsorption was more effective. The negative value in the change of Gibb's free energy revealed that the adsorption is spontaneous and feasible at 20 – 40 ˚C.

In accordance with the Bio-Circular-Green (BCG) business model, agricultural waste is the starting material that cannot be overlooked. Each agricultural waste has unique properties that should be explored and enhanced. Turmeric waste is a biomass residue that currently lacks monetary value but is abundant, inexpensive, and provides ease of collection. The obtained activated carbon has high mesopore volume which is desirable in emerging pollutant adsorption. Futher work could explore the adsorption capacity of other pollutants.

จุฬาลงกรณ์มหาวิทยาลัย
Chulalongkorn University

Nomenclature

S_{BET} (m^2/g)	is the BET surface area.
V_{mic} (cm^3/g)	is the micropore volume.
V_{meso} (cm^3/g)	is the mesopore volume.
V_T (cm^3/g)	is the total pore volume.
q_e (mg/g)	is Norfloxacin uptake at equilibrium.
C_0 (mg/l)	is the initial concentration of Norfloxacin.
C_e (mg/l)	is the Norfloxacin concentration at equilibrium.
V (l)	is the volume of solution.
W (mg)	is the weight of the adsorbent.
K_L (l/mg)	is the Langmuir isotherm constant.
q_m (mg/g)	is the maximum monolayer adsorption capacity.
R_L	is the separation factor from Langmuir isotherm.
K_F $(mg/g)(1/mg)^{1/n}$	is the Freundlich isotherm constant.
n	is a dimensionless term regarding the magnitude of surface heterogeneity.
q_{DR} (mg/g)	is the D-R adsorption capacity.
K_{DR} (mol^2/kJ^2)	is a constant related to the adsorption energy.
ε	is the Polanyi potential.
q_t (mg/g)	is the amount of NOR uptake at a given time t,

จุฬาลงกรณ์มหาวิทยาลัย
CHULALONGKORN UNIVERSITY

C_t (mg/l)	is the remaining concentration of adsorbate at time t,
k_1 (1/min)	is the PFO rate constant.
q_{e1} (mg/g)	is the amount of NOR adsorbed at equilibrium according to the PFO model.
k_2 (g/mg·min)	is the PSO rate constant.
q_{e2} (mg/g)	is the amount of NOR adsorbed at equilibrium according to the PSO model.
h (mg/g·min)	is the initial rate of adsorption.
α (mg/g·min)	is the initial adsorption rate.
β (g/mg)	is the desorption constant.
k_i (mg/g·$min^{1/2}$)	is the IPD constant.
Ci (mg/g)	is the y-intercept of the regression and IPD constant associated with the film thickness.
R (J/mol·K)	is the gas constant (8.314 J/mol·K).
T (K)	is the temperature.
ΔG (kJ/mol)	is the change in Gibb's free energy.
ΔH (kJ/mol)	is the change in enthalpy.
ΔS (J/mol·K)	is the change in entropy.
t (min)	is time.
g	is gram.
mg	is milligram.

จุฬาลงกรณ์มหาวิทยาลัย
Chulalongkorn University

l	is litre.
min	is minute.
h	is hour.
m^2	is square metre.
rpm	is round per minute.
ml	is millilitre.
nm	is nanometre.
μm	is micrometre.
°C	is degree Celsius.
mol	is mole.
J	is Joule.

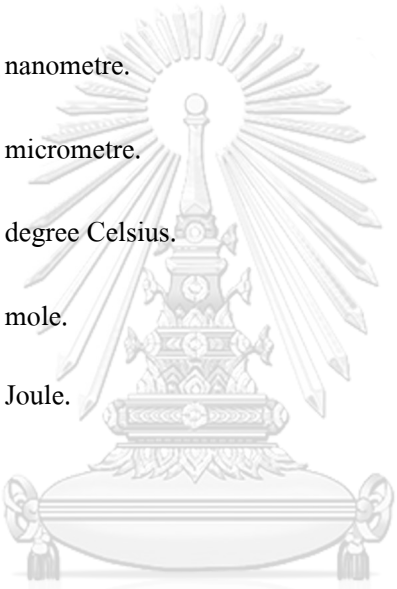

จุฬาลงกรณ์มหาวิทยาลัย
Chulalongkorn University

Appendix

Cellulose, hemicellulose, lignin compositions of turmeric waste

Raw turmeric waste (TW) received from the extraction factory was analyzed for lignocellulosic compositions as shown in Table 18.

Table 18 Lignocellulosic composition of turmeric waste

Compound	Composition (%w/w)	Method
Cellulose	58.77	HPLC (Column: VertiSep™ LMP)
Hemicellulose	1.24	HPLC (Column: VertiSep™ LMP)
Lignin	11.63	NREL/TP-510-42618
Total	71.64	

Activated carbon yield

The carbonization yield was determined by the following equation:

$$\%\text{yield} = \frac{m_{in} - m_{out}}{m_{in}} \times 100 \quad (21)$$

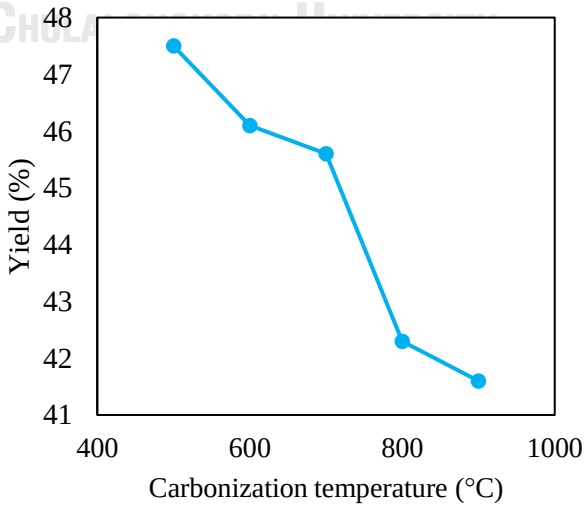

Figure 32 Yield percentage of TWAC500 - 900 at different carbonization temperature

Fig. 31 shows the yield percentage of TWAC500 – 900 which is a decreasing at higher carbonization temperature because of more volatile matter removal.

Statistical tool

In this work, the coefficient of determination (R^2) is the chosen statistical tool, the equation is written in eq (22). The closer R^2 value is to 1, the better the experimental data fit with that particular model.

$$R^2 = 1 - \frac{SSR}{SST} = 1 - \frac{\sum_i (y_i - \hat{y}_i)^2}{\sum_i (y_i - \bar{y})^2} \quad (22)$$

where R^2 is the coefficient of determination,

SSR is the sum of squares residuals,

SST is the total sum of squares,

y_i is the experimental data,

$\hat{y}_i$ is the calculated value,

$\bar{y}$ is the mean of all experimental values.

BET equation for BET surface area calculation [77]

$$\frac{P}{V(P_0 - P)} = \frac{1}{V_m C} + \frac{(C-1)P}{V_m C P_0} \quad (23)$$

where P is the equilibrium pressure (atm),

P_0 is the saturation pressure (atm),

V is the volume of adsorbed gas (cm^3),

V_m is the volume of monolayer adsorbed gas (cm^3),

C is the BET constant related to the adsorption heat in the monolayer (q_1) and the heat of condensation (q_L) ($C \approx \exp[(q_L - q_1)/RT)]$),

To calculated BET surface area, a linear regression of y-axis [$P/(V(P-P_0))$] and x-axis P/P0 was plotted. The BET surface area was calculated in range $0.05 < P/P_0 < 0.30$. The y-intercept is $1/(V_mC)$ while the slope is $(C - 1)/(V_mC)$.

$$S_{total} = \frac{V_m N_s}{V} \tag{24}$$

$$S_{BET} = \frac{S_{total}}{a} \tag{25}$$

where S_{total} is the total surface area of the sample (cm^3),

S_{BET} is the BET surface area (cm^3/g),

N_s is the Avogadro's number,

a is the weight of the sample (g).

DR for micropore calculation [78]

$$\frac{W}{W_0} = \exp\left[-\frac{\left[RT\ln\left(\frac{P_0}{P}\right)\right]^2}{(\beta E_0)^2}\right] \tag{26}$$

where W is the weight of the adsorbed gas at P/P_0 and T (g),

W_0 is the total weight adsorbed (g),

T is the temperature 77 K,

R is the gas constant,

P is the equilibrium pressure (atm),

P_0 is the saturation pressure (atm),

E_0 is a characteristic energy that depends on the adsorbent,

β is the scaling factor.

จุฬาลงกรณ์มหาวิทยาลัย
Chulalongkorn University

BJH for mesopore parallel pore (H3 hysteresis loop) and pore distribution [79]

$$d_p = 2(r_k + t) \quad (27)$$

$$r_k = -\frac{0.2082}{\log\left(\frac{P}{P_0}\right)} \quad (28)$$

$$t = 0.354\left(\frac{-5}{\ln\left(\frac{P}{P_0}\right)}\right)^{1/3} \quad (29)$$

where d_p is the actual diameter of the pore (nm),

r_k is the Kelvin radius of the pore (nm),

t is the thickness of the adsorbed film (nm) calculated from Halsey equation,

P is the equilibrium pressure (atm),

P_0 is the saturation pressure (atm).

Point of zero charge

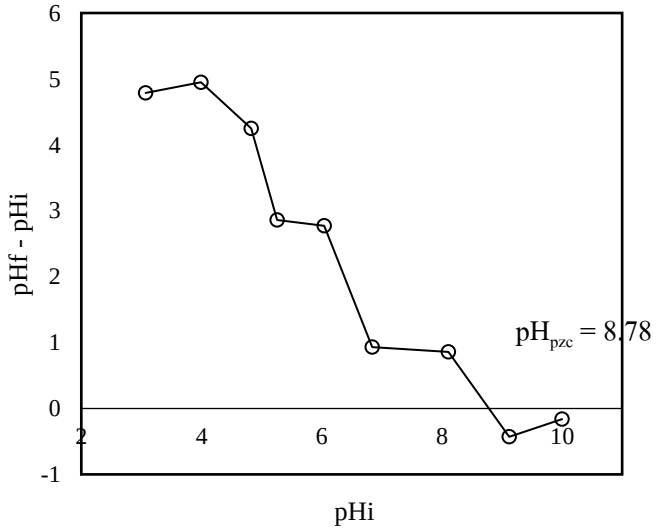

Figure 33 Initial pH and change in pH plot to determine pH_{pzc} of TWAC700

From Fig. 32 it can be concluded that pH_{pzc} of TWAC700 is 8.78. For pH solution less than 8.78, the surface of TWAC700 was positively charged, whereas beyond pH 8.78, the surface was negatively charged.

UV-Visible spectroscopy

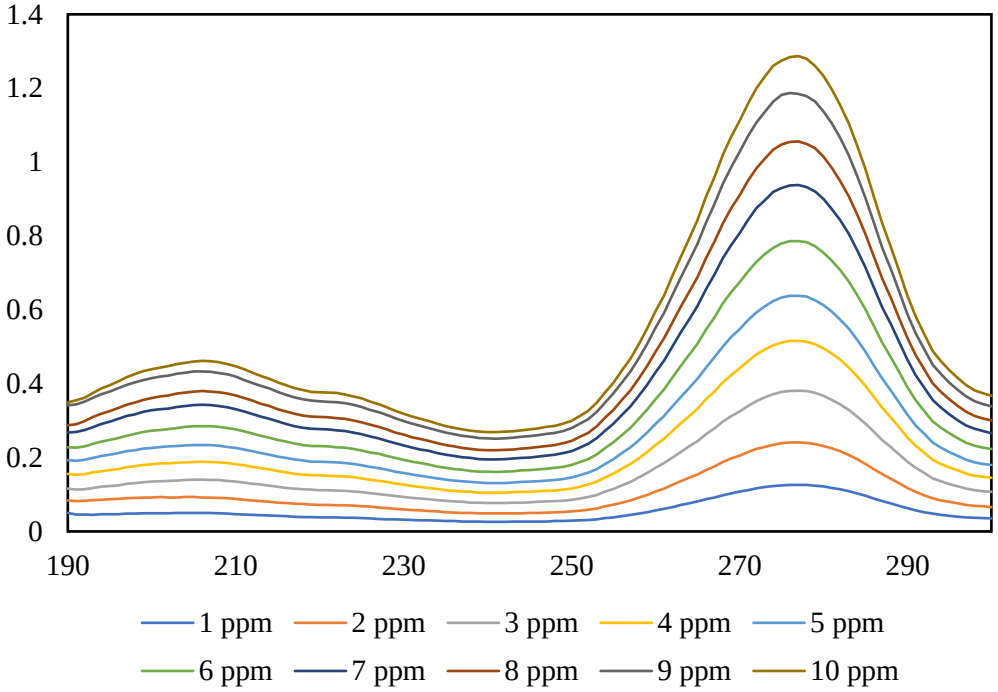

Figure 34 UV-Visible absorbance spectrum of standard NOR solution 1-10 mg/l

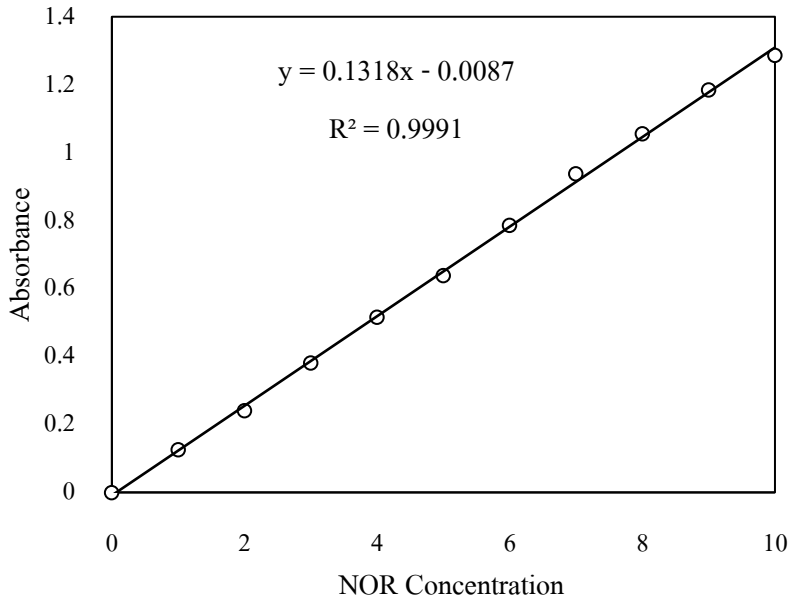

Figure 35Calibration plot of Norfloxacin concentration and absorbance at wavelength 277 nm

Comparative adsorption capacities of TWAC500 – 900 and TWB700

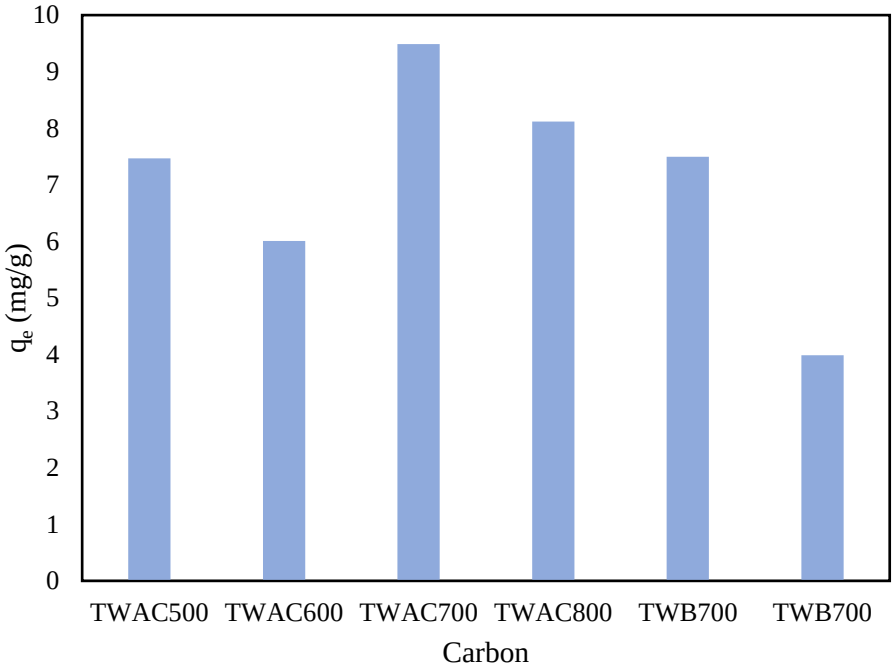

Figure 36 q_e of NOR adsorption using TWAC500-900 and TWB700 at C_0 = 25 mg/l

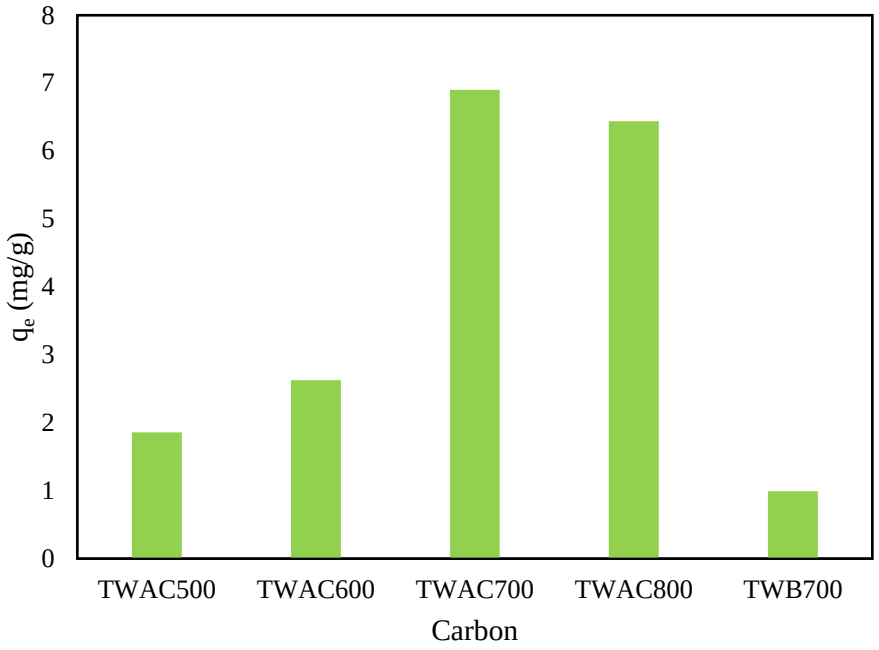

Figure 37 q_e of NOR adsorption using TWAC500-800 and TWB700 at C_0 = 10 mg/l

Adsorption supplementary data

Table 19 Effect of carbon dosage, 25 °C, 200 rpm, 24 h (section 4.3.1)

Carbon (g)	C_i (mg/l)	C_e (mg/l)	%removal	q_e (mg/g)
0.0251	8.79	4.44	49.5	17.3
0.0503	8.79	3.72	57.6	10.1
0.0998	8.79	1.93	78.1	6.88
0.2000	8.79	0.768	91.3	4.01
0.2999	8.79	0.639	92.7	2.72

Table 20 Effect of initial concentration and equilibrium of adsorption, 25 °C, 200 rpm, 24 h (section 4.3.2 – 4.3.3)

Carbon (g)	C_i (mg/l)	C_e (mg/l)	%removal	q_e (mg/g)
0.1000	8.98	3.10	65.5	5.88
0.1007	14.9	6.63	55.5	8.27
0.1000	20.2	10.6	47.4	9.56
0.1001	29.9	16.5	44.7	13.4
0.1000	40.4	24.0	40.5	16.4
0.0999	62.7	41.3	34.1	21.4
0.1000	78.1	54.2	30.6	23.9
0.1000	111	80.0	28.2	31.4
0.1000	150	117	22.1	33.0
0.1000	180	146	18.8	33.8
0.1000	196	162	17.1	33.5

สถาบันวิทยบริการ
จุฬาลงกรณ์มหาวิทยาลัย
CHULALONGKORN UNIVERSITY

Table 21 Adsorption kinetics 25 °C, 200 rpm (section 4.3.4)

t (min)	Carbon (g)	V (ml)	C_t (mg/l)	q_t (mg/g)
4	0.1000	100	29.7	3.56
6	0.1000	100	28.9	4.43
8	0.1000	100	27.5	5.81
10	0.1005	100	39.1	7.28
20	0.1003	100	36.2	10.2
40	0.1005	98	35.6	10.8
60	0.1003	98	35.6	11.7
90	0.1005	96	34.7	12.0
240	0.1003	96	34.4	14.2
300	0.1000	96	25.4	14.4
480	0.1000	96	25.2	15.6
1140	0.1000	100	24.0	15.2
1440	0.0999	100	24.4	15.6
2880	0.0997	98	29.2	16.2
4320	0.0999	96	24.9	16.4

จุฬาลงกรณ์มหาวิทยาลัย
CHULALONGKORN UNIVERSITY

Table 22 Thermodynamics of adsorption, 200 rpm, 24 h (section 4.3.5)

Temperature (°C)	Carbon (g)	C_e (mg/l)	q_e (mg/g)
20	0.0996	8.00	10.0
20	0.1005	21.7	18.3
20	0.0999	43.0	22.9
20	0.1008	60.5	25.9
30	0.0994	10.5	9.43
30	0.0999	28.3	15.6
30	0.0994	42.5	18.6
30	0.1009	65.5	22.2
40	0.1011	13.8	6.4
40	0.099	26.6	13.4
40	0.1011	49.5	16.4
40	0.1011	68.5	19.2

จุฬาลงกรณ์มหาวิทยาลัย
CHULALONGKORN UNIVERSITY

REFERENCES

จุฬาลงกรณ์มหาวิทยาลัย
Chulalongkorn University

1. Roberts, S.C. and T.R. Zembower, *Global increases in antibiotic consumption: a concerning trend for WHO targets.* The Lancet Infectious Diseases, 2021. **21**(1): p. 10-11.
2. Nada, A.H., et al., *Comparative bioavailability of norfloxacin tablets based on blood and urine data.* Med Princ Pract, 2007. **16**(6): p. 426-31.
3. เศวตโยธิน, ว., การปนเปื้อนของสารกลุ่มผลิตภัณฑ์ยาและผลิตภัณฑ์ดูแลสุขภาพในแม่น้ำบางปะ กง. กรมส่งเสริมคุณภาพสิ่งแวดล้อม:กรุงเทพฯ, 2016.
4. Bartoskova, M., et al., *Norfloxacin—Toxicity for Zebrafish Focused on Oxidative Stress Parameters.* BioMed Research International, 2014. **2014**: p. 560235.
5. Department of Agriculture extension, ขมิ้นชัน: ปีเพาะปลูก *2561*, in ระบบจัดเก็บและรายงานข้อมูลภาวการณ์ผลิตพืชรายเดือน ระดับตำบล (รต.). 2019.
6. Board, N.H. *Volume of turmeric produced across India in financial year 2018, by state*. [Website] 2019 [cited 2021]; Available from: https://www.statista.com/statistics/870963/turmeric-production-by-state-india/.
7. ช่างทา, ช., คุณประโยชน์และฤทธิ์ทางชีวภาพที่หลากหลายของสมุนไพรขมิ้นชัน. วารสารวิทยาศาสตร์และเทคโนโลยี หัวเฉียวเฉลิมพระเกียรติ, 2015. **1**(2): p. 94-109.
8. comtrade, U. *Leading turmeric exporting countries worldwide in 2019*. 2020; Available from: https://www.statista.com/statistics/798287/main-turmeric-export-countries-worldwide/.
9. Gopi, S., et al., *Isolation and characterization of stable nanofiber from turmeric spent using chemical treatment by acid hydrolysis and its potential as antimicrobial and antioxidant activities.* Journal of Macromolecular Science, Part A, 2019. **56**(4): p. 327-340.
10. Gopi, S., et al., *Bionanocomposite films based on potato, tapioca starch and chitosan reinforced with cellulose nanofiber isolated from turmeric spent.* Journal of the Taiwan Institute of Chemical Engineers, 2019. **96**: p. 664-671.
11. Wang, F., et al., *Effects of antibiotic norfloxacin on the degradation and enantioselectivity of the herbicides in aquatic environment.* Ecotoxicology and Environmental Safety, 2021. **208**: p. 111717.
12. (NDI), N.D.I., Thailand National List of Essential Medicines (NLEM), 2020.

จุฬาลงกรณ์มหาวิทยาลัย
CHULALONGKORN UNIVERSITY

13. Geissen, V., et al., *Emerging pollutants in the environment: A challenge for water resource management.* International Soil and Water Conservation Research, 2015. **3**(1): p. 57-65.

14. Arman, N.Z., et al., *A Review on Emerging Pollutants in the Water Environment: Existences, Health Effects and Treatment Processes.* Water, 2021. **13**(22): p. 3258.

15. Li, C., et al., *Synergistic effects of anionic surfactants on adsorption of norfloxacin by magnetic biochar derived from furfural residue.* Environmental Pollution, 2019. **254**: p. 113005.

16. Alnajjar, A., A.M. Idris, and H.H. AbuSeada, *Development of a stability-indicating capillary electrophoresis method for norfloxacin and its inactive decarboxylated degradant.* Microchemical Journal, 2007. **87**(1): p. 35-40.

17. Baralla, E., et al., *An Overview of Antibiotics as Emerging Contaminants: Occurrence in Bivalves as Biomonitoring Organisms.* Animals, 2021. **11**(11): p. 3239.

18. หวังเกียรติ, อ., ยาในสิ่งแวดล้อม ภัยเงียบที่คุกคาม. ยาวิพากษ์, 2018. **9**(37): p. 3-7.

19. Qin, T., et al., *A novel biochar derived from cauliflower (Brassica oleracea L.) roots could remove norfloxacin and chlortetracycline efficiently.* Water Science and Technology, 2017. **76**(12): p. 3307-3318.

20. Vieno, N., T. Tuhkanen, and L. Kronberg, *Elimination of pharmaceuticals in sewage treatment plants in Finland.* Water Research, 2007. **41**(5): p. 1001-1012.

21. Fick, J., et al., *Contamination of surface, ground, and drinking water from pharmaceutical production.* Environmental Toxicology and Chemistry, 2009. **28**(12): p. 2522-2527.

22. Kairigo, P., et al., *Contamination of Surface Water and River Sediments by Antibiotic and Antiretroviral Drug Cocktails in Low and Middle-Income Countries: Occurrence, Risk and Mitigation Strategies.* Water, 2020. **12**(5): p. 1376.

23. Li, W., et al., *Investigation of antibiotics in mollusks from coastal waters in the Bohai Sea of China.* Environmental Pollution, 2012. **162**: p. 56-62.

24. Xie, H., et al., *Pharmaceuticals and personal care products in water, sediments, aquatic organisms, and fish feeds in the Pearl River Delta: Occurrence, distribution, potential*

จุฬาลงกรณ์มหาวิทยาลัย
CHULALONGKORN UNIVERSITY

sources, and health risk assessment. Science of The Total Environment, 2019. **659**: p. 230-239.

25. Tell, J., et al., *Science-based Targets for Antibiotics in Receiving Waters from Pharmaceutical Manufacturing Operations.* Integrated Environmental Assessment and Management, 2019. **15**(3): p. 312-319.
26. Pan, Y., et al., *Lethal/sublethal responses of Daphnia magna to acute norfloxacin contamination and changes in phytoplankton-zooplankton interactions induced by this antibiotic.* Scientific Reports, 2017. **7**(1): p. 40385.
27. Sui, M., et al., *Adsorption of norfloxacin in aqueous solution by Mg–Al layered double hydroxides with variable metal composition and interlayer anions.* Chemical Engineering Journal, 2012. **210**: p. 451-460.
28. *Compound summary: Norfloxacin*. [cited] 2022; Available from: https://pubchem.ncbi.nlm.nih.gov/compound/Norfloxacin.
29. Giorno, L., E. Piacentini, and F. Bazzarelli, *Macroporous, Mesoporous, and Microporous Membranes*, in *Encyclopedia of Membranes*, E. Drioli and L. Giorno, Editors. 2016, Springer Berlin Heidelberg: Berlin, Heidelberg. p. 1-2.
30. Chen, H., et al., *Cotton derived carbonaceous aerogels for efficient removal of organic pollutants and heavy metal ions.* J. Mater. Chem. A, 2015. **3**.
31. Hu, L., et al., *Hemicellulose-Based Polymers Processing and Application.* American Journal of Plant Sciences, 2020. **11**: p. 2066-2079.
32. Lu, Y., et al., *Structural Characterization of Lignin and Its Degradation Products with Spectroscopic Methods.* Journal of Spectroscopy, 2017. **2017**: p. 8951658.
33. Basu, P., *Chapter 5 - Pyrolysis*, in *Biomass Gasification, Pyrolysis and Torrefaction (Third Edition)*, P. Basu, Editor. 2018, Academic Press. p. 155-187.
34. Bhaskar, T., et al., *Chapter 3 - Thermochemical Conversion of Biomass to Biofuels*, in *Biofuels*, A. Pandey, et al., Editors. 2011, Academic Press: Amsterdam. p. 51-77.
35. Heidarinejad, Z., et al., *Methods for preparation and activation of activated carbon: a review.* Environmental Chemistry Letters, 2020. **18**(2): p. 393-415.
36. Angin, D., *Production and characterization of activated carbon from sour cherry stones by zinc chloride.* Fuel, 2014. **115**: p. 804-811.

จุฬาลงกรณ์มหาวิทยาลัย
CHULALONGKORN UNIVERSITY

37. Sanchez, J., *Characterization of activated carbon produced from coffee residues by chemical and physical activation*. Masters thesis, KTH Chemical Science and Engineering, Stockholm, 2011.

38. Tran, H.N., et al., *Mistakes and inconsistencies regarding adsorption of contaminants from aqueous solutions: A critical review.* Water Research, 2017. **120**: p. 88-116.

39. Ayawei, N., A.N. Ebelegi, and D. Wankasi, *Modelling and Interpretation of Adsorption Isotherms.* Journal of Chemistry, 2017. **2017**: p. 3039817.

40. Wang, J. and X. Guo, *Adsorption isotherm models: Classification, physical meaning, application and solving method.* Chemosphere, 2020. **258**: p. 127279.

41. Weber, T.W. and R.K. Chakravorti, *Pore and solid diffusion models for fixed-bed adsorbers.* AIChE Journal, 1974. **20**(2): p. 228-238.

42. Foo, K.Y. and B.H. Hameed, *Insights into the modeling of adsorption isotherm systems.* Chemical Engineering Journal, 2010. **156**(1): p. 2-10.

43. Sahoo, T.R. and B. Prelot, *Chapter 7 - Adsorption processes for the removal of contaminants from wastewater: the perspective role of nanomaterials and nanotechnology*, in *Nanomaterials for the Detection and Removal of Wastewater Pollutants*, B. Bonelli, et al., Editors. 2020, Elsevier. p. 161-222.

44. Borhan, A., et al., *Characterization and Modelling Studies of Activated Carbon Produced from Rubber-Seed Shell Using KOH for CO2 Adsorption.* Processes, 2019. **7**(11): p. 855.

45. Weber, W.J. and J.C. Morris, *Kinetics of adsorption on carbon from solution.* Journal of the sanitary engineering division, 1963. **89**(2): p. 31-60.

46. Karthikeyan, S., P. Sivakumar, and P. Palanisamy, *Novel activated carbons from agricultural wastes and their characterization.* Journal of Chemistry, 2008. **5**(2): p. 409-426.

47. Santhosh, P., A. Sridevi, and C. Dhandapani, *Studies on the removal of acid blue 25 from wastewater using activated carbon and turmeric (Curcuma longa L.) as adsorbent.* Nature Environment and Pollution Technology, 2013. **12**: p. 331-335.

48. Wang, Z., et al., *Norfloxacin Sorption and Its Thermodynamics on Surface-Modified Carbon Nanotubes.* Environmental Science & Technology, 2010. **44**(3): p. 978-984.

จุฬาลงกรณ์มหาวิทยาลัย
CHULALONGKORN UNIVERSITY

49. Wang, B., et al., *Preparation of biochar by simultaneous carbonization, magnetization and activation for norfloxacin removal in water.* Bioresource Technology, 2017. **233**: p. 159-165.

50. Yang, W., et al., *Adsorption behavior and mechanisms of norfloxacin onto porous resins and carbon nanotube.* Chemical Engineering Journal, 2012. **179**: p. 112-118.

51. Liu, W., et al., *Sorption of norfloxacin by lotus stalk-based activated carbon and iron-doped activated alumina: Mechanisms, isotherms and kinetics.* Chemical Engineering Journal, 2011. **171**(2): p. 431-438.

52. Chen, W., et al., *Efficient adsorption of Norfloxacin by Fe-MCM-41 molecular sieves: Kinetic, isotherm and thermodynamic studies.* Chemical Engineering Journal, 2015. **281**: p. 397-403.

53. Wang, J., et al., *Adsorption characteristics and mechanism of norfloxacin in water by γ-Fe2O3@BC.* Water Science and Technology, 2020. **82**(2): p. 242-254.

54. Luo, J., et al., *Sorption of norfloxacin, sulfamerazine and oxytetracycline by KOH-modified biochar under single and ternary systems.* Bioresource Technology, 2018. **263**: p. 385-392.

55. Yang, X., et al., *Mechanistic insights into removal of Norfloxacin from water using different natural iron ore – biochar composites: more rich free radicals derived from natural pyrite-biochar composites than hematite-biochar composites.* Applied Catalysis B: Environmental, 2019. **255**: p. 117752.

56. Liu, P., et al., *Sorption of Sulfadiazine, Norfloxacin, Metronidazole, and Tetracycline by Granular Activated Carbon: Kinetics, Mechanisms, and Isotherms.* Water, Air, & Soil Pollution, 2017. **228**(4): p. 129.

57. Feng, Y., et al., *Norfloxacin removal from aqueous solution using biochar derived from luffa sponge.* Journal of Water Supply: Research and Technology-Aqua, 2018. **67**(8): p. 703-714.

58. Fu, H., et al., *Activated carbon adsorption of quinolone antibiotics in water: Performance, mechanism, and modeling.* Journal of Environmental Sciences, 2017. **56**: p. 145-152.

จุฬาลงกรณ์มหาวิทยาลัย
CHULALONGKORN UNIVERSITY

59. Swinehart, D.F., *The Beer-Lambert Law.* Journal of Chemical Education, 1962. **39**(7): p. 333.

60. Zhao, C., E. Jiang, and A. Chen, *Volatile production from pyrolysis of cellulose, hemicellulose and lignin.* Journal of the Energy Institute, 2017. **90**(6): p. 902-913.

61. Leng, E., et al., *Effect of KCl and CaCl2 loading on the formation of reaction intermediates during cellulose fast pyrolysis.* Proceedings of the Combustion Institute, 2017. **36**(2): p. 2263-2270.

62. Leng, E., et al., *In situ evolution of functional groups in char during cellulose pyrolysis under the catalysis of KCl and CaCl2.* Fuel, 2022. **309**: p. 122227.

63. Phothong, K., C. Tangsathitkulchai, and P. Lawtae, *The Analysis of Pore Development and Formation of Surface Functional Groups in Bamboo-Based Activated Carbon during CO2 Activation.* Molecules, 2021. **26**(18): p. 5641.

64. Brunner, P.H. and P.V. Roberts, *The significance of heating rate on char yield and char properties in the pyrolysis of cellulose.* Carbon, 1980. **18**(3): p. 217-224.

65. Xue, Y., et al., *Relationship of cellulose and lignin contents in biomass to the structure and RB-19 adsorption behavior of activated carbon.* New Journal of Chemistry, 2018. **42**(20): p. 16493-16502.

66. Cagnon, B., et al., *Contributions of hemicellulose, cellulose and lignin to the mass and the porous properties of chars and steam activated carbons from various lignocellulosic precursors.* Bioresource Technology, 2009. **100**(1): p. 292-298.

67. Ahmed, M.J. and S.K. Theydan, *Physical and chemical characteristics of activated carbon prepared by pyrolysis of chemically treated date stones and its ability to adsorb organics.* Powder Technology, 2012. **229**: p. 237-245.

68. Li, W., et al., *Synthesis and structure regulation of armor-wearing biomass-based porous carbon: Suppression the leakage current and self-discharge of supercapacitors.* Carbon, 2022. **196**: p. 136-145.

69. Ma, F., et al., *Sakura-based activated carbon preparation and its performance in supercapacitor applications.* RSC advances, 2019. **9**(5): p. 2474-2483.

จุฬาลงกรณ์มหาวิทยาลัย
CHULALONGKORN UNIVERSITY

70. Siyasukh, A., Y. Chimupala, and N. Tonanon, *Preparation of magnetic hierarchical porous carbon spheres with graphitic features for high methyl orange adsorption capacity.* Carbon, 2018. **134**: p. 207-221.

71. Saka, C., *BET, TG–DTG, FT-IR, SEM, iodine number analysis and preparation of activated carbon from acorn shell by chemical activation with ZnCl2.* Journal of Analytical and Applied Pyrolysis, 2012. **95**: p. 21–24.

72. Alahabadi, A., et al., *Comparing adsorption properties of NH4Cl-modified activated carbon towards chlortetracycline antibiotic with those of commercial activated carbon.* Journal of Molecular Liquids, 2017. **232**: p. 367-381.

73. Wang, F.Y., H. Wang, and J.W. Ma, *Adsorption of cadmium (II) ions from aqueous solution by a new low-cost adsorbent—Bamboo charcoal.* Journal of Hazardous Materials, 2010. **177**(1): p. 300-306.

74. Feng, C., et al., *Graphene/waste-newspaper cellulose composite aerogels with selective adsorption of organic dyes: preparation, characterization, and adsorption mechanism.* New Journal of Chemistry, 2020. **44**(6): p. 2256-2267.

75. Hu, Zhonghua & Srinivasan, Madapusi & Ni, Yaming. *Novel Activation Process for Preparing Highly Microporous and Mesoporous Activated Carbons.* Carbon, 2001. **39**: p. 877-886.

76. *Carbokarn Grades*. [cited] 2022; Available from: https://www.carbokarn.co.th/en/activated-carbon-basics/

77. Rodríguez-Reinoso, F. and A. Sepúlveda-Escribano, *Chapter 9 - POROUS CARBONS IN ADSORPTION AND CATALYSIS*, in *Handbook of Surfaces and Interfaces of Materials*, H.S. Nalwa, Editor. Academic Press: Burlington, 2001. p. 309-355.

78. Saeidi, N., Parvini, M. *Accuracy of Dubinin-Astakhov and Dubinin-Radushkevich Adsorption Isotherm Models in Evaluating Micropore Volume of Bentonite*, Periodica Polytechnica Chemical Engineering, 2016. **60**(2): p. 123–129.

79. Izabel C. Medeiros-Costa, Catherine Laroche, Javier Pérez-Pellitero, Benoit Coasne, *Characterization of hierarchical zeolites: Combining adsorption/intrusion, electron microscopy, diffraction and spectroscopic techniques*, Microporous and Mesoporous Materials, 2019. **287**: p. 167-176.

จุฬาลงกรณ์มหาวิทยาลัย
CHULALONGKORN UNIVERSITY

จุฬาลงกรณ์มหาวิทยาลัย
Chulalongkorn University

VITA

NAME	Nuttamon Vanichsetakul
DATE OF BIRTH	13 January 1997
PLACE OF BIRTH	Bangkok
INSTITUTIONS ATTENDED	Department of Chemical Engineering, Faculty of Engineering, Chulalongkorn University
HOME ADDRESS	99/44 Serithai Rd, Khannayao, Khannayao, Bangkok 10230

จุฬาลงกรณ์มหาวิทยาลัย
CHULALONGKORN UNIVERSITY